https://doi.org/10.5194/egusphere-2026-742
Preprint. Discussion started: 23 February 2026

A Reanalysis of the Arctic sea ice cover over the satellite era utilising summertime observations of SIT

Nicholas Williams[1, 2], Nicholas Byrne[3], Daniel Feltham[1], Peter Jan Van Leeuwen[4], Ross Bannister[3], David Schroeder[1], Isobel Lawrence[5], Lars Nerger[6], Jack Landy[7], and Geoffrey Dawson[8]

[1]Centre for Polar Observation and Modelling, Department of Meteorology, University of Reading, Earley Gate, PO Box 243, Reading, RG6 6BB, UK
[2]Nansen Environmental and Remote Sensing Center (NERSC), Bergen, Norway
[3]Department of Meteorology, University of Reading, Earley Gate, PO Box 243, Reading, RG6 6BB, UK
[4]Department of Atmospheric Science, Colorado State University, Fort Collins, CO 80523, United States
[5]Centre for Polar Observation and Modelling, Department of Geography and Environmental Science, Northumbria University, Newcastle, UK
[6]Alfred Wegener Institute, Helmholtz Centre for Polar and Marine Research, Bremerhaven, Germany
[7]Centre for Integrated Remote Sensing and Forecasting for Arctic Operations, Department of Physics and Technology, University of Tromsø: The Arctic University of Norway, Norway
[8]University of Bristol, School of Geographical Sciences, Bristol BS8 1SS, UK

Correspondence: Nicholas Williams (nicholas.williams@nersc.no)

Abstract.

Climate change has significantly affected the Arctic over the satellite era, with sea ice undergoing a substantial decline. While changes in sea ice concentration (SIC) and sea ice extent (SIE) have been widely studied, sea ice thickness (SIT) and volume (SIV) remain less well constrained due to limited observations. Quantifying SIV trends is particularly important for understanding sea ice changes in response to climate change. Here we present three reanalyses that assimilate different combinations of SIC and SIT products, including year-round SIT observations, into the CPOM-CICE sea ice model, which incorporates advanced parameterisations for melt ponds, form drag, and rheology. Assimilating NASA Team SIC together with year-round SIT substantially improves SIT estimates, and year-round SIT assimilation outperforms winter-only SIT assimilation, even at the end of winter, by better initialising the growth season. Comparison with four independent observational datasets and PIOMAS identifies the best-performing reanalysis, which we analyse for 2010–2020 to diagnose model deficiencies. The model exhibits a seasonally compensating bias cycle: excessive freeze-up and overly thick, consolidated ice in autumn and winter lead to elevated extent and thickness and a suppressed marginal ice zone in spring, while enhanced late-summer melt offsets these errors, yielding September extents close to observations but with anomalously thick ice packed against the Canadian Arctic Archipelago. This suggests that misrepresentations of ice growth, lead formation and refreezing, marginal ice zone dynamics, mechanical redistribution, and melt timing interact to obscure errors in concentration and thickness. Additionally, our best performing reanalysis also shows the thickest ice is less thick and more evenly distributed across the central Arctic in the 2010s. This reanalysis provides new insight into recent Arctic sea ice change and its underlying processes, as well as identifying key deficiencies in the sea ice model physics which can be a focus for future model development.

https://doi.org/10.5194/egusphere-2026-742
Preprint. Discussion started: 23 February 2026

1 Introduction

Arctic sea ice is a major component of the global climate system; it interacts with the surrounding atmosphere and ocean through exchanges of heat, moisture and momentum, driving changes in both the local and global climate. The Arctic has experienced the effects of human-induced climate change more than any other region on Earth. Arctic Amplification (AA) has seen the Arctic warm at a rate 3-5 times faster than the global average since 1979 (Rantanen et al., 2022). AA is driven by sea ice loss caused by rising atmospheric carbon dioxide levels from anthropogenic emissions (Notz and Stroeve, 2016; Dai et al., 2019). Since 1979, Arctic sea ice cover has declined at an average rate of approximately 5% per decade, with an accelerated decrease in the 21st century (Cavalieri and Parkinson, 2012). The global impacts of Arctic climate change and the mechanisms driving these shifts are still being investigated (Francis et al., 2017; Eayrs et al., 2021; Riihelä et al., 2021; Previdi et al., 2021; Schuur et al., 2022). Advancing our understanding of the physical processes behind these changes is crucial for Arctic communities (Arruda and Krutkowski, 2017), wildlife (David et al., 2016; Hunter et al., 2010), and shipping (Melia et al., 2016; Min et al., 2022; Shu et al., 2024).

Over the past 15 years, the Arctic sea ice cover has shifted from being dominated by thick multi-year ice (MYI) to thinner, seasonal first-year ice (FYI), with MYI extent declining by roughly 50% (Kwok, 2018; Stroeve et al., 2014; Stroeve and Notz, 2018). Consequently, accurately representing the physical properties of FYI and its interactions with the ocean and atmosphere has become increasingly critical for modelling the Arctic sea ice system. This transition has driven greater focus on the marginal ice zone (MIZ)—the dynamic ice-edge region where waves strongly influence sea ice behaviour (Strong et al., 2017). Recent advances include the introduction of floe size distribution schemes (Bateson et al., 2020), the coupling of sea ice and wave models (Boutin et al., 2020), and discrete-element rheologies to better capture sea ice drift and deformation (Rampal et al., 2015). Despite this progress, substantial uncertainties remain in the representation of rheology, ice–ocean momentum exchange, and wave–ice feedbacks, as MIZ processes overall act as a negative feedback in winter, but are positive in summer (Horvat, 2022; Bennetts et al., 2022; Frew et al., 2025). Moreover, recent evaluations show that thermodynamic processes in CMIP6 sea ice models are systematically overestimated compared with buoy observations (West and Blockley, 2024). These gaps raise key questions about when, where, and why models misrepresent melt and growth, and the relative roles of FYI and MYI in these processes. To address these issues, we develop a reanalysis of the Arctic sea ice cover that integrates state-of-the-art modelling with satellite observations of sea ice concentration (SIC) and thickness (SIT) to provide a spatially and temporally consistent record over the past four decades.

In comparison with the atmosphere and ocean, there are relatively fewer reanalysis studies focusing on sea ice. One reason for this is a lack of available observations for assimilation with good spatial and temporal coverage in comparison with the rest of the globe. The first studies combining data assimilation and sea ice appeared in the early-mid 1990s, with the assimilation of SIC (Thomas and Rothrock, 1993; Thomas et al., 1996). The Pan-Arctic Ice Ocean Modeling and Assimilation System (PIOMAS) reanalysis was first introduced in 2003 by Zhang and Rothrock (2003). PIOMAS is a coupled ice-ocean

https://doi.org/10.5194/egusphere-2026-742
Preprint. Discussion started: 23 February 2026

model which assimilates sea surface temperature (SST) data in ice-free grid cells, and ice concentration, using a relatively simple nudging technique, which aims to move the model variables closer to their observed counterparts by use of a weighting factor. PIOMAS has been extensively validated and is often used for validating Arctic sea ice in models, reanalyses and observations (Schweiger et al., 2011). Another prominent reanalysis focusing on sea ice is the TOPAZ4 system (Sakov et al., 2012). This is also a coupled ocean-ice model which assimilates (alongside ocean parameters) ice concentration and ice drift, and also has successfully implemented SIT assimilation from the combined CryoSat-2 and Satellite Moisture and Ocean Salinity (CS2SMOS) dataset (Ricker et al., 2017; Xie et al., 2018). There are now a wide number of operational ocean-sea ice reanalysis and prediction systems (Chevallier et al., 2017), with the majority only assimilating SIC alongside ocean variables like sea surface temperature (SST), temperature and salinity.

The launch of CryoSat-2 (CS2) (Wingham et al., 2006) has since allowed the processing of SIT observations since October 2010 with good spatial and temporal coverage and high accuracy. The two ice thickness datasets most often used for assimilation have been the Centre for Polar Observation and Modelling (CPOM) dataset (Laxon et al., 2013), and the Alfred Wegener Institute (AWI) dataset, which combines thicker ice measurements from CS2 with thinner ice measurements from the Soil Moisture and Salinity (SMOS) radiometer (Ricker et al., 2017). In the past 5-10 years there have been a number of studies assimilating ice thickness data derived from this satellite. Blockley and Peterson (2018) assimilated the Laxon et al. (2013) SIT dataset using optimal interpolation (OI) using the UK Met Office's FOAM/GloSea 5, and has since assimilated along-track daily SIT data using 3D-Var (Fiedler et al., 2022), and showed positive results for prediction and reanalysis in validation with independent data. Xie et al. (2018), assimilated the AWI CS2SMOS SIT into the TOPAZ4 system using an Ensemble Kalman Filter (EnKF) method and reduced both bias and errors against validation data. Fritzner et al. (2019) compared the assimilation of SIC, CPOM CS2 SIT and a snow depth product (Rostosky et al., 2018) in a short reanalysis study using a coupled ocean-sea ice system and an EnKF, and found that ice thickness assimilation can improve SIC, thickness and snow depth. A study by Mu et al. (2020) using a fully coupled climate model (Alfred Wegener Institute, Helmholtz Center for Polar and Marine Research Climate Model (AWI-CM, v1.1)) showed that assimilating SIT improved estimates of SIT in comparison to the Beaufort Gyre Exploration Project (BGEP) upward looking sonar (ULS) mooring SIT data (Krishfield et al., 2014). Recently, a new year-round dataset of SIT was developed from the CS2 observations using machine learning and produced in Landy et al. (2022). Min et al. (2023) assimilated this dataset into the Massachusetts Institute of Technology general circulation model (MITgcm) and showed that it can improve estimates of Arctic SIT. Zhang et al. (2023) showed that year-round SIT resulted in strong improvements in September sea ice prediction. Recently it has also been shown that assimilation of a sea ice thickness distribution (SITD) can improve model estimates of sea ice (Williams et al., 2023). Other studies highlighting the benefits of SIT assimilation include Yang et al. (2014); Massonnet et al. (2015); Mu et al. (2018); Mignac et al. (2022); Nab et al. (2025); Williams et al. (2025). In summary, assimilation of SIT data clearly shows strong benefits for both prediction and reanalysis in climate modelling.

We present a new data assimilation system that combines the CPOM implementation of the Los Alamos Sea Ice Model (CICE)

https://doi.org/10.5194/egusphere-2026-742
Preprint. Discussion started: 23 February 2026

(Hunke et al., 2015) with the Parallelised Data Assimilation Framework (PDAF) (Nerger et al., 2005). Using this framework, we produce three different reanalyses over the satellite era (1981–2020) assimilating different configurations of SIC, SIT, and SITD, including recent year-round SIT observations (Landy et al., 2022). These reanalyses provide new insights into long-term changes in sea ice cover, allow systematic evaluation of model performance during the CryoSat-2 era (2010–present), and highlight key directions for improving sea ice modelling. Independent validation is carried out using Operation IceBridge (OIB), Beaufort Gyre Exploration Project (BGEP) upward-looking sonar (ULS) SIT data, and a withheld subset of winter CryoSat-2 observations.

This study is outlined as follows. In section 2 we outline the sea ice model and data assimilation scheme used to produce the reanalysis, the observational datasets used for assimilation in the reanalyses, and the data used to validate the reanalyses. We also discuss validation metrics for our reanalyses. In section 3 we first present a validation of our reanalysis with independent SIT observations. We then present key results from our sea ice reanalysis including sea ice concentration, extent, thickness, volume and their trends and climatology. We then compare our best performing reanalysis against a free run of our model CPOM-CICE, highlighting key differences between the two, identifying the causes and the possible deficiencies in the model, and possible methods to resolve them in the model physics. In section 4 the results are discussed in further detail. In the conclusion we discuss the key results, outcomes and potential future works.

2 Method

2.1 CPOM-CICE

We use a standalone sea ice model, the CPOM version of the CICE model v5.1.2 (CPOM-CICE), which uses five thickness categories (lower limits 0 m, 0.6 m, 1.2 m, 2.4 m and 3.6 m). This includes an internal stress tensor with an elastic-plastic-anisotropic rheology (Tsamados et al., 2013) in the sea ice momentum balance, which matches observations better than other often-used sea ice rheologies, and also parameterisations for form drag (Tsamados et al., 2014). The horizontal transport equation is solved using the incremental remapping scheme of Lipscomb and Hunke (2004). The transport of sea ice in thickness space is determined by the remapping scheme of Lipscomb (2001), where its mechanical redistribution is formulated by the scheme of Lipscomb et al. (2007) with ice strength defined as in Rothrock (1975). The 1-dimensional vertical Bitz and Lipscomb (Bitz and Lipscomb, 1999) thermodynamical model is used to solve the ice and snow heat flux equations in each category and accounts for the freezing and melting of brine pockets. The topographic melt pond scheme of Flocco et al. (2010) is used. The natural optical properties of the snow and ice are better accounted for by using a Delta-Eddington approach (Briegleb and Light, 2007) to define their scattering and absorption characteristics for computing the sea ice shortwave albedo and incoming shortwave radiation. This is used in conjunction with the bubbly brine thermal conductivity parameterisation (Pringle et al., 2007), which increases the conductivity of colder sea ice.

CICE is a dynamic and thermodynamic model of sea ice designed to function as the sea ice component of a fully coupled

https://doi.org/10.5194/egusphere-2026-742
Preprint. Discussion started: 23 February 2026

global climate model, but in this study we use it standalone, not coupled to any atmospheric or ocean climate model. The CPOM-CICE model has previously been used to produce realistic estimates of the sea ice state using the parameterisations described in this section (Schröder et al., 2019; Rolph et al., 2020; Bateson et al., 2020). We use the thermodynamic slab mixed layer ocean model with a prognostic ocean temperature contained within CICE which is initialised with ocean temperature and salinity from a climatology based on an ocean reanalysis (Ferry et al., 2011). The prognostic ocean temperature is restored to the monthly climatology with a 20 day timescale to account for heat advection in the ocean. The mixed layer salinity is also prescribed from the same climatology. The ocean currents (also at 3 m depth) are also taken from the same reanalysis. The atmospheric forcing data used are NCEP-2 (Kanamitsu et al., 2002) comprising daily downward shortwave and longwave radiation fluxes and 6-hourly 2 m temperature and humidity and 10 m wind velocity. These atmospheric forcing fields are perturbed to generate ensemble spread as described in (Williams et al., 2023). We also take monthly mean precipitation from the same reanalysis, which is not perturbed. We run CPOM-CICE on the ORCA 1 degree tripolar grid over a pan-Arctic domain.

2.2 Ensemble Kalman Filter

In this work, we couple CPOM-CICE to the Parallel Data Assimilation Framework (PDAF) (Nerger and Hiller, 2013), a software environment that provides efficient ensemble-based data assimilation for climate models with minimal modifications to the original model code. We use PDAF version 1.16, which offers a modular implementation supporting numerous observation types and simplifies assimilation compared to earlier versions. Data assimilation is performed using the Local Ensemble Transform Kalman Filter (LETKF) (Hunt et al., 2007). The LETKF is a sequential data assimilation method that estimates the mean and covariance of the posterior probability density function (PDF), assuming Gaussian error statistics, rather than solving for the posterior mode as in variational methods. Errors are assumed to be unbiased and Gaussian. Localisation is applied to mitigate spurious long-distance correlations arising from ensemble undersampling. In this study, a Gaspari–Cohn function (Gaspari and Cohn, 1999) is used for covariance localisation, which smoothly decreases to zero at the specified localisation radius. A localisation radius of 200 km is used in all reanalyses. The LETKF also supports ensemble spread maintenance through the use of inflation or a forgetting factor (Pham et al., 1998). A forgetting factor of 0.995 (equivalent to an inflation factor of 1.01) is used in this study, which we previously applied successfully in this system (Williams et al., 2023).

2.3 Observations for Assimilation

In this study we assimilate SIC daily data from either the Bootstrap (Comiso, 2017) dataset or the NASA Team (Cavalieri and Parkinson, 2012). These datasets are available daily from 1979 to the present. These datasets are not assimilated together but in two separate reanalysis experiments. These datasets use different SIC retrieval algorithms but are based upon the same principle, only differing in choices of frequency channels, polarisations and reference brightness temperatures (Ivanova et al., 2014). The two datasets generally show similar ice-edge positions in the Arctic (Comiso et al., 1997), though the NASA Team dataset has lower ice concentrations around the outer regions of the ice pack. Fluctuations in the ice pack can also produce discrepancies which may lead to large differences in SIC retrieval between the two datasets (Comiso et al., 1997). One key difference is in how the two algorithms handle melt ponds, which appear as open water in the satellite data. The Bootstrap al-

https://doi.org/10.5194/egusphere-2026-742
Preprint. Discussion started: 23 February 2026

gorithm tries to offset this bias by synthetically increasing estimates of SICs much more than the Team algorithm does (Bunzel et al., 2018). In our reanalyses we compare and contrast the assimilation of NASA Team and Bootstrap SIC data with regards to the different effects their assimilation has on the estimates of the Arctic sea ice state.

Errors on SIC estimates from satellites are difficult to quantify, but overall retrieval accuracy is estimated to be between 5% and 10%. The largest errors can arise in the marginal ice zone (MIZ), and in summer where melt ponds can dominate the surface of the sea ice cover (Ivanova et al., 2015), in these grid cells errors may be as high as 30% (Comiso, 2017). In this paper, we use observation errors for the SIC that depend on the season and the observed ice concentration. For SIC measurements above 0.8, we use an observation error of 0.2 for May-September (inclusive), and 0.1 outside of these months. Otherwise we use an observation error of 0.15. The same observation error is used for each dataset.

The second type of observation we assimilate in this study is SIT. The first SIT dataset we use is the year-round SIT dataset of (Landy et al., 2022), also derived from CS2 radar altimetry measurements (hereafter referred to as AYR-CS2). Previously, Arctic SIT datasets were often limited to the winter months due to the presence of melt ponds on the ice surface during spring and summer. Within conventional satellite (radar) processing routines, these melt ponds are interpreted as leads, precluding an accurate estimation of ice freeboard (Laxon et al., 2013; Ricker et al., 2017) Landy et al. (2022) follows on work by Dawson et al. (2022), which uses a trained 1D convolutional neural network to separate CS2 radar returns from leads with those from floes and melt ponds. In Landy et al. (2022), this work is continued by converting the estimated freeboard to thickness, and importantly correcting for a thickness bias in the CS2 radar altimeter. This bias in the CS2 radar altimeter causes an underestimation of the thickest ice in the central Arctic, and is corrected for by assessing the radar response over melt pond covered sea ice and simulations to characterise the electromagnetic response. The bias-corrected freeboard measurements are then converted to ice thickness using snow depths and densities from a Lagrangian snow loading model. The SIT measurements are averaged and produced on 80 km grid cell size at 15 day intervals, we have interpolated these into monthly mean SIT estimates on the ORCA 1 degree tripolar grid. The SIT measurements calculated in May and September have patterns that closely resemble the April and October WIN-CS2 CPOM processed SIT respectively. Individual error statistics are provided with each observation, which are used for the observation error covariance matrix for the assimilation. Observation errors for this product are lower in winter and higher in summer. We assimilate monthly averages of SIT in the middle of each month as an instantaneous observation. This dataset is available in bi-weekly and monthly periods from October 2010 to the present.

The second SIT dataset we use is the winter CS2 SIT dataset Laxon et al. (2013); Tilling et al. (2018) (we refer to this dataset as WIN-CS2 from hereon). As with AYR-CS2, this dataset is available from October 2010, but only between October and April. There are two key processes in producing SIT measurements from the raw observation data: the differentiation between measurements of surface elevation of the ocean and surface elevation of the sea ice, and the process which then converts the calculated freeboard to thickness. Sea ice and the leads between ice floes can be differentiated in radar echoes by the shape of the echo waveform, and then a process known as retracking is used to determine the location on each waveform which

https://doi.org/10.5194/egusphere-2026-742
Preprint. Discussion started: 23 February 2026

represents the average surface elevation within the satellite footprint. CPOM uses a Gaussian-plus-exponential waveform fit to retrack echoes from leads (Giles et al., 2008) and a 70% leading edge threshold from the first peak to retrack floe echoes (Tilling et al., 2018). Other retrackers have been used to produce freeboard and thickness data from CS2, which can yield markedly different results (Ricker et al., 2014). It is assumed that the radar bursts reflect off the snow-ice interface as shown in Beaven (1995) though more recent research shows that this may not always be the case (Stroeve et al., 2020). The biggest source of uncertainty occurs when converting freeboard to SIT, assuming hydrostatic equilibrium. This requires knowledge of the snow cover on the Arctic, which is extremely limited. WIN-CS2 uses a modified Warren climatology, derived from measurements from Soviet drifting stations between 1954-1991 (Warren et al., 1999). The climatological snow depth is halved over FYI, in line with results from airborne field campaigns (Kurtz and Farrell, 2011). Due to the uncertainties in the retracking and conversion of freeboard to thickness, uncertainty is highest in the thinner measurements of ice for WIN-CS2. Therefore we do not use thickness measurements of ice thickness below 0.5 m. As with AYR-CS2, WIN-CS2 is assimilated as a monthly average in the middle of each month. Errors are not provided with the product, and are estimated as in Williams et al. (2023). We use a randomly withheld 25% subset of the total data for validation, the other 75% of which is assimilated.

The final observation assimilated is the SITD derived from CS2, first assimilated in Williams et al. (2023). The dataset is derived from CS2 measurements, so is only available in winter, and as with SIT data, we assimilate monthly averages in the middle of each month. SITD observations are derived from the individual observations of thickness from the WIN-CS2 dataset. These individual measurements are binned according to the thickness distribution used in our CICE model (Schröder et al., 2019), with measurements over one month used to find monthly mean values. We then have observations of ten different variables; a_n^*, the area of ice (as a proportion of the total ice) in categories 1-5, where the open water fraction a_0 in that grid cell is unknown, and h_n, the mean thickness of ice in categories 1-5. For a_n^* this means

$$\sum_{n=1}^{5} a_n^* = 1.$$

These observed variables are related to the state variables a_n and v_n by

$$a_n = a_n^* a$$
$$h_n = \frac{v_n}{a_n},$$

where a is the total fraction of sea ice in a grid cell, a_n is the fraction of sea ice in thickness category n in a grid cell and v_n is the volume of ice per unit grid cell area in category n. The uncertainties on these observations are very difficult to ascertain due to the processing of the product and the multiple sources of contributing errors in the processing. We use the same error

https://doi.org/10.5194/egusphere-2026-742
Preprint. Discussion started: 23 February 2026

analysis as in Williams et al. (2023) to find reasonable estimates of errors which we summarise briefly here. It is difficult to find errors for ice concentration and ice thickness in each category that are consistent with all estimated values of mean ice thickness (which use relative errors). However we find that using a total error of 0.3 for ice concentration in each category and 0.8 m for ice thickness in each category leads at least to errors that are close to (or slightly worse than) the mean ice thickness error equivalent. The derivation of these errors is described in more detail in Williams et al. (2023). Note that the SITD is only assimilated together with the Laxon et al. (2013) WIN-CS2 SIT dataset from which it is derived, not the AYR-CS2 dataset.

2.4 Observations for Validation

We use four datasets for validation in this paper. The first is the OIB SIT quick-look dataset between 2011 and 2016 (Kurtz et al., 2013). As the more reliable Level 4 product (Kurtz et al., 2016) does not cover the whole period of our assimilation experiment. We also use the quick-look version 1 dataset (Kurtz et al., 2015) for evaluation. The OIB dataset consists of observations from the Advanced Topographic Laser Altimeter (ATLAS) flown on airborne missions during surveys done in March-April each year between 2009-2019 (We use the L4 product data for 2011-2013, and the L1 quick-look data between 2014-2016). The aircraft fly at an altitude of 460 m, use along track smoothing of 40 m and an observation frequency corresponding to 1 m along-track. This oversampling allows for statistical smoothing (Farrell et al., 2011). The OIB SIT data are at a much higher resolution than our model, so are averaged daily and interpolated onto the ORCA 1 degree tripolar grid.

The second dataset of SIT observations we use for validation are the sea ice drafts, the thickness of the sea ice under sea level, from the BGEP moorings. BGEP includes ULS measuring instruments Krishfield et al. (2014). There are a total of 4 moorings, 2 of which (A and B) have been in operation since August 2003, C was in operation until 2008, and D has been in operation since 2005. The ULS instruments measured sea ice draft every 2 seconds before 2014, and every second after. The sea ice draft is found by subtracting the range measured by the ULS instrument from the known depth of the instrument. The draft measurements have a stated error of 5-10 cm (Krishfield and Proshutinsky, 2006). To compare this data to our model monthly mean thickness, we first take the monthly means of the sea ice draft observations. We convert the sea ice draft into SIT using the method of Rothrock et al. (2008), using hydrostatic equilibrium and accounting for seasonal changes in snow depth using the Warren climatology (Warren et al., 1999), and then average all the measurements over each month to find the monthly mean thicknesses which we can compare to the model. If a month has more than 3 days consecutive missing data, then we do not calculate a monthly average for that month.

The final dataset we use is PIOMAS (Zhang and Rothrock, 2003) SIT and SIV. This is for validation and comparison with our own reanalyses. PIOMAS is a sea ice and ocean reanalysis running from 1979 to the present day. PIOMAS assimilates SIC using a relatively simple nudging technique which moves the model variables closer to their observed counterparts. PIOMAS also assimilates SST through optimal interpolation (OI). PIOMAS has been extensively validated through in-situ (submarine, ship and mooring) and satellite observations, with its uncertainty in SIV for October calculated to be 1.35×10^3 km^3 (Schweiger

https://doi.org/10.5194/egusphere-2026-742
Preprint. Discussion started: 23 February 2026

et al., 2011), as an example. Due to this extensive validation, PIOMAS is often used as a validation and comparison tool for sea ice datasets.

2.5 Validation Metrics

In this paper we use a variety of metrics to understand and validate the reanalysis. We define SIE as the sum of the area where ice concentration is 15% or greater. We use bias, RMSE and Pearson's correlation coefficient as follows

$$\text{Bias} = \sum_{i=1}^{N} W_i(x_i - y_i), \tag{1}$$

$$\text{RMSE} = \sqrt{\sum_{i=1}^{N} W_i(x_i - y_i)^2}, \tag{2}$$

$$\text{Correlation} = \frac{\sum_{i=1}^{N} x_i' y_i'}{\sqrt{\sum_{i=1}^{N} x_i'^2}\sqrt{\sum_{i=1}^{N} y_i'^2}}, \tag{3}$$

where x_i and y_i are the model and observation values respectively, N is the total number of data points. W_i are weights proportional to the area of the corresponding grid cell. For point-wise bias and RMSE calculations W_i is $\frac{1}{N}$, x_i' and y_i' are the residuals between the model/observation values and their respective means. We additionally use a simple linear regression (line of best fit) to evaluate our reanalyses and CPOM-CICE against the validation datasets.

2.6 Experimental Setup

The reanalyses are setup as follows: There is a four year spin-up phase beginning in 1977, with the CPOM-CICE model running in ensemble mode to allow for the spinning up of the CICE model and for the generation of an ensemble spread that will be sufficient for the ensemble Kalman filter to reasonably account for the model error. All reanalyses are run with 100 ensemble members using a newly generated set of atmospheric forcing fields, with an amplification factor α (Williams et al., 2023) of 1.25, a localisation radius of 200 km and a forgetting factor of 0.995. The reanalysis period spans from January 1981 to April 2020 with SIC assimilated bi-daily from 1981 to 1989, and daily thereafter. AYR-CS2 SIT is assimilated monthly in the middle of the month from October 2010. We run three configurations of the reanalysis, assimilating different combinations of Bootstrap SIC observations, NASA Team SIC observations and CS2 SIT. The free (or control) run is known as CPOM-CICE. The reanalysis system is known as CPOM Arctic Sea Ice Reanalysis (CASIRA), with the three different reanalyses referred to as CASIRA-n (assimilating NASA Team SIC and AYR-CS2), CASIRA-b (assimilating Bootstrap SIC and AYR-CS2) and CASIRA-d (assimilating NASA Team SIC, WIN-CS2 and SITD). As the errors in the NASA Team and Bootstrap products are believed to be similar we use the same observation errors when assimilating the two products (see section 2.3). All other parameters in the assimilation system are also the same. The configurations of these reanalyses are detailed in table 1.

https://doi.org/10.5194/egusphere-2026-742
Preprint. Discussion started: 23 February 2026

Table 1. Configurations of the control run and three different reanalyses produced in this paper. SIC refers to sea ice concentration assimilation, SIT refers to sea ice thickness assimilation and SITD refers to sea ice thickness distribution assimilation. N indicates no assimilation of this product takes place.

Experiment	SIC assimilated	SIT assimilated	SITD assimilated
CPOM-CICE	None	None	None
CASIRA-b	Bootstrap	AYR-CS2	None
CASIRA-n	NASA Team	AYR-CS2	None
CASIRA-d	NASA Team	WIN-CS2	SITD

3 Results

3.1 Model Validation

In this section, we corroborate and compare the reanalyses with independent SIT observations from the OIB mission, the Beaufort Gyre Exploration Project (BGEP) upward-looking-sonar (ULS) moorings, and the WIN-CS2 SIT observations withheld from assimilation. A statistical comparison with each of these datasets is shown in Table 2, and each dataset is further compared below.

The OIB dataset is re-gridded onto the ORCA 1 degree tripolar grid and we then compare the coincident SIT data from OIB with our reanalyses and WIN-CS2, shown in Figure 1. CPOM-CICE shows a strong linear fit with the coincident OIB data, with values of 0.42 and 0.42 respectively, whereas the reanalyses have lower linear slope fits. This is because higher OIB SIT measurements (above 3 m) fit better to CPOM-CICE and WIN-CS2 SIT at those locations, whereas the reanalyses contain thinner ice. The correlations are similar between all the products, lying between 0.5 and 0.6. However the RMSEs are substantially lower for the reanalyses in comparison with CPOM-CICE and WIN-CS2. As high SIT measurements from OIB appear to correlate much better with WIN-CS2 and CPOM-CICE, it shows the reanalyses have much better estimates of sea ice between 1 m and 3 m thick than CPOM-CICE and WIN-CS2.

A comparison with the four BGEP ULS moorings, which provide greater temporal coverage of Arctic sea ice changes throughout the 21st century, is a better comparison than OIB for long term changes in sea ice, though spatial coverage is much more limited. Figure 2 and Table 2 show that CASIRA-n consistently compares best with the four BGEP ULS moorings throughout the time period for moorings A and B, with much higher correlations and much lower RMSEs in comparison to CPOM-CICE and CASIRA-b. For moorings C and D however, it has slightly higher RMSEs than CPOM-CICE (though still lower than CASIRA-n and CASIRA-b), yet still higher correlations than CPOM-CICE. All moorings are located in the Beaufort Sea, but moorings A and B are located further from the Canadian Arctic Archipelago (CAA) and closer to the Chukchi Sea, within the Beaufort Sea (the mooring locations are shown in Figure 12a)). Overall, CASIRA-n is the best performing model in comparison to the BGEP ULS dataset.

https://doi.org/10.5194/egusphere-2026-742
Preprint. Discussion started: 23 February 2026

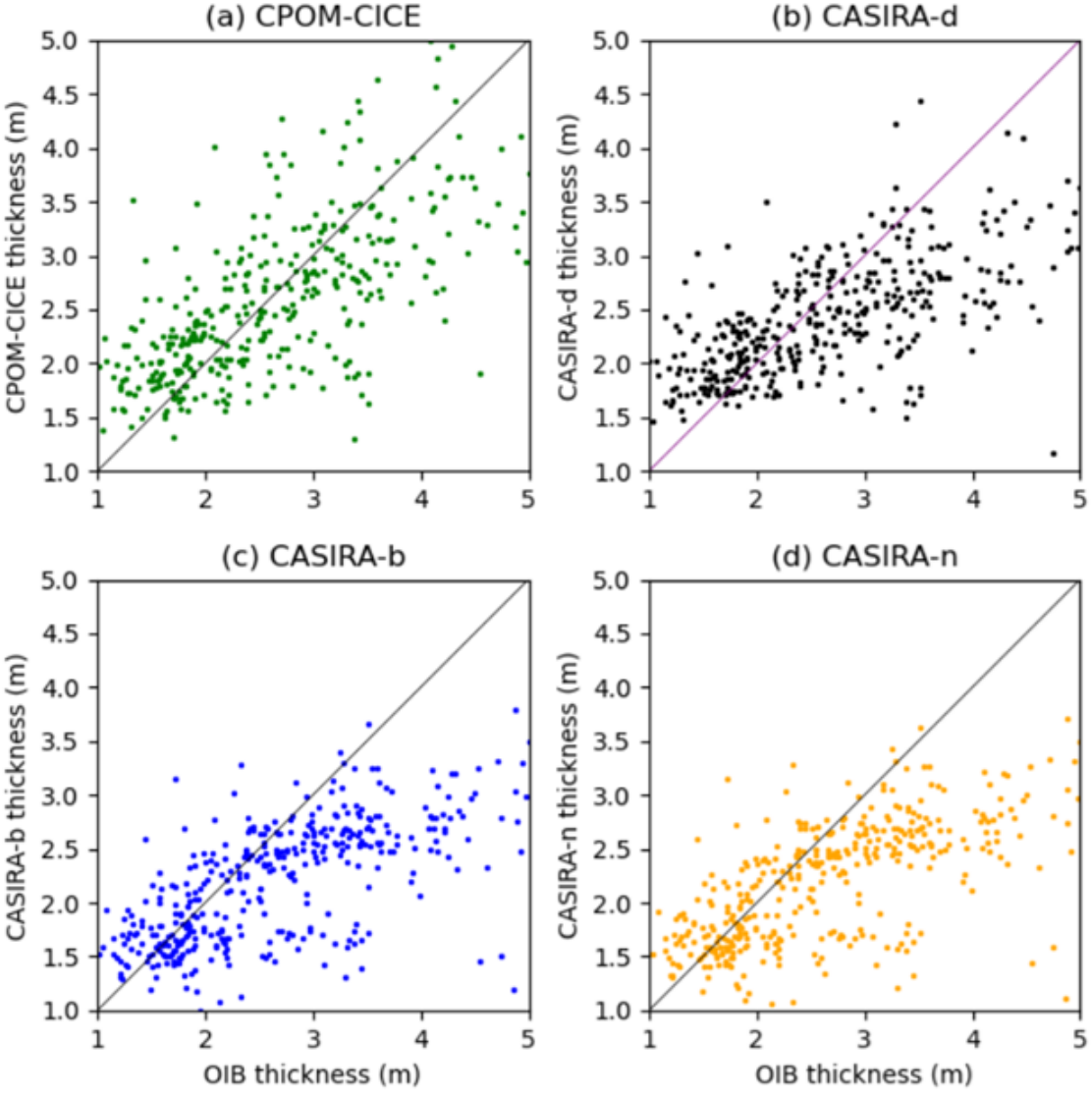

Figure 1. Scatter plot of coincident SIT data between OIB and ensemble mean CPOM-CICE, CASIRA-d, CASIRA-b, CASIRA-n for the missions from 2011-2015. The diagonal black lines show y=x for reference.

https://doi.org/10.5194/egusphere-2026-742
Preprint. Discussion started: 23 February 2026

WIN-CS2	Correlation	RMSE	Linear Regression
CPOM-CICE	0.51	1.02	-0.35
CASIRA-b	0.62	0.38	0.07
CASIRA-n	**0.66**	**0.20**	**-0.03**
CASIRA-d	0.64	0.28	-0.10
OIB	Correlation	RMSE	Linear Regression
CPOM-CICE	0.52	0.54	0.47
CASIRA-b	0.56	0.30	0.36
CASIRA-n	**0.57**	**0.29**	0.36
CASIRA-d	0.47	0.39	**0.30**
WIN-CS2	0.51	0.47	0.42

BGEP ULS	A-Correlation	A-RMSE	B-Correlation	B-RMSE	C-Correlation	C-RMSE	D-Correlation	D-RMSE
CPOM-CICE	0.85	0.61	0.84	0.59	0.76	**0.49**	0.64	**0.38**
CASIRA-b	0.74	0.97	0.73	0.91	**0.87**	0.7	0.82	0.45
CASIRA-n	**0.92**	**0.30**	**0.88**	**0.32**	**0.87**	0.59	**0.85**	0.45
CASIRA-d	0.90	0.36	0.85	0.39	**0.87**	0.63	**0.85**	**0.38**

Table 2. RMSE, correlation and linear Regression for CPOM-CICE, CASIRA-b, CASIRA-n and CASIRA-d against WIN-CS2, OIB and BGEP ULS moorings A, B, C and D. The best performing model run for each metric and each comparison dataset are shown in bold.

The final dataset we compare our reanalyses to is the WIN-CS2 SIT. We compare it to a randomly withheld 25% subset of the total data, the other 75% of which is assimilated in CASIRA-d. This dataset is derived from the same raw satellite data as AYR-CS2 (though the processing differs substantially) - so these are not comparisons of completely independent dataset - but it can still serve as a useful validation tool. In Figure 3 the density plots show that CPOM-CICE can have much higher SIT than WIN-CS2 at ice thicknesses higher than 2.5 m. CASIRA-b and CASIRA-n show a slight underestimate of SIT higher than 2.5 m compared to WIN-CS2, and slight overestimate of ice thicknesses under 2.5 m. CASIRA-b and CASIRA-N have slightly better correlations to WIN-CS2 than CPOM-CICE (Table 2), and much improved fitted linear slopes and RMSE. CASIRA-n shows the strongest reduction in RMSE, substantially reduced from both CPOM-CICE and CASIRA-b.

Overall there is substantial improvement in SIT estimates of our reanalyses compared to the control run, particularly after 2010, but we also have some comparisons in BGEP and OIB containing pre-2010 data, which is promising for the period in the reanalyses when only SIC assimilation takes place. CASIRA-n is particularly promising, as it is the best performing reanalysis for correlation, reduced RMSE and better linear fits in 11 out of 14 cases (see Table 2). It is particularly notable

https://doi.org/10.5194/egusphere-2026-742
Preprint. Discussion started: 23 February 2026

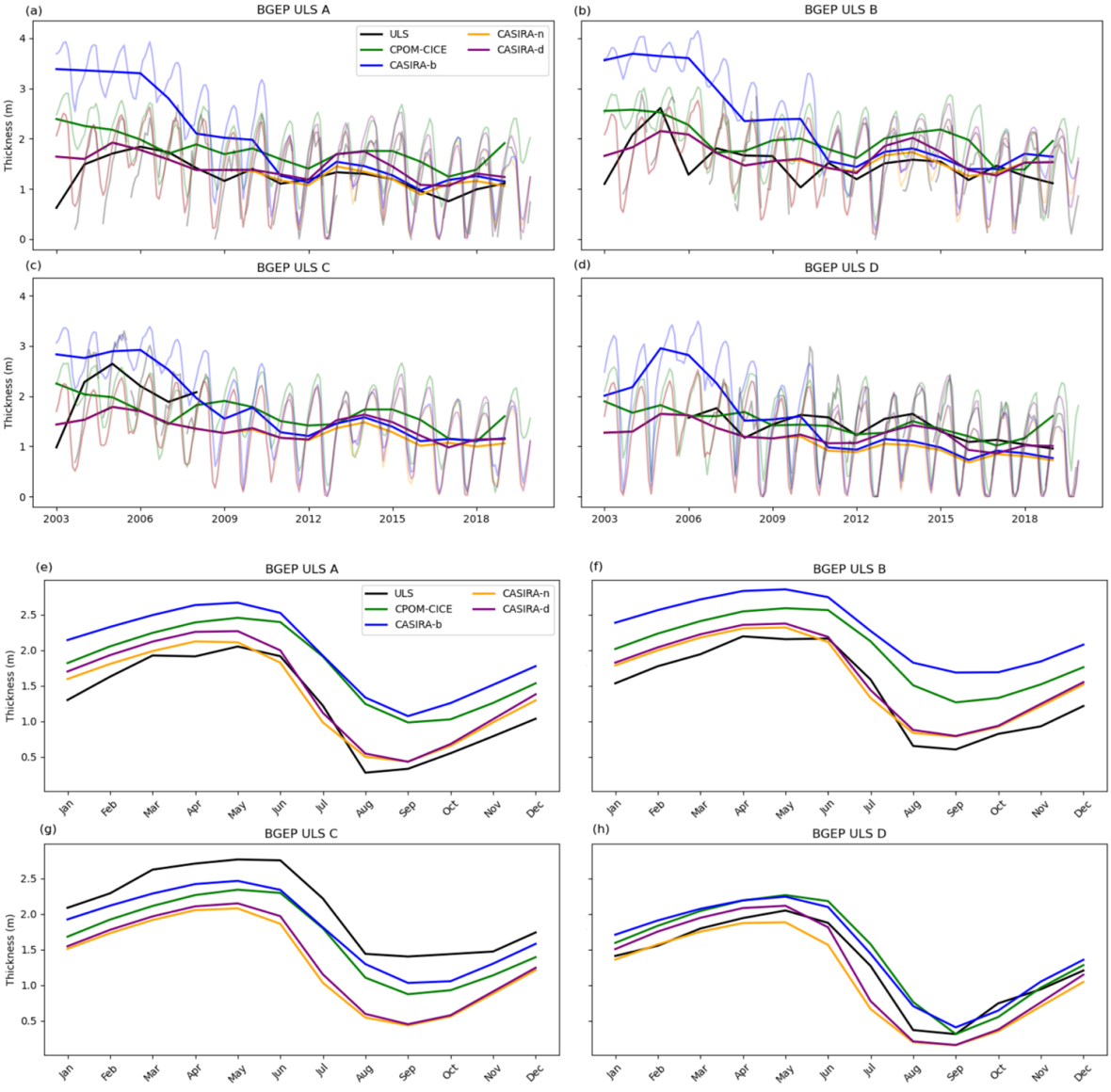

Figure 2. Top (a-d): Yearly (opaque) and monthly (partially transparent) averages of SIT from the ULS instruments and the coincident monthly mean SIT averaged across ensemble members from CPOM-CICE, CASIRA-d, CASIRA-b and CASIRA-n between 2003 and 2020. Bottom (e-h): Monthly climatology of SIT averaged across ensemble members from BGEP ULS, CPOM-CICE, CASIRA-d, CASIRA-b and CASIRA-n for each month between 2003-2020.

https://doi.org/10.5194/egusphere-2026-742
Preprint. Discussion started: 23 February 2026

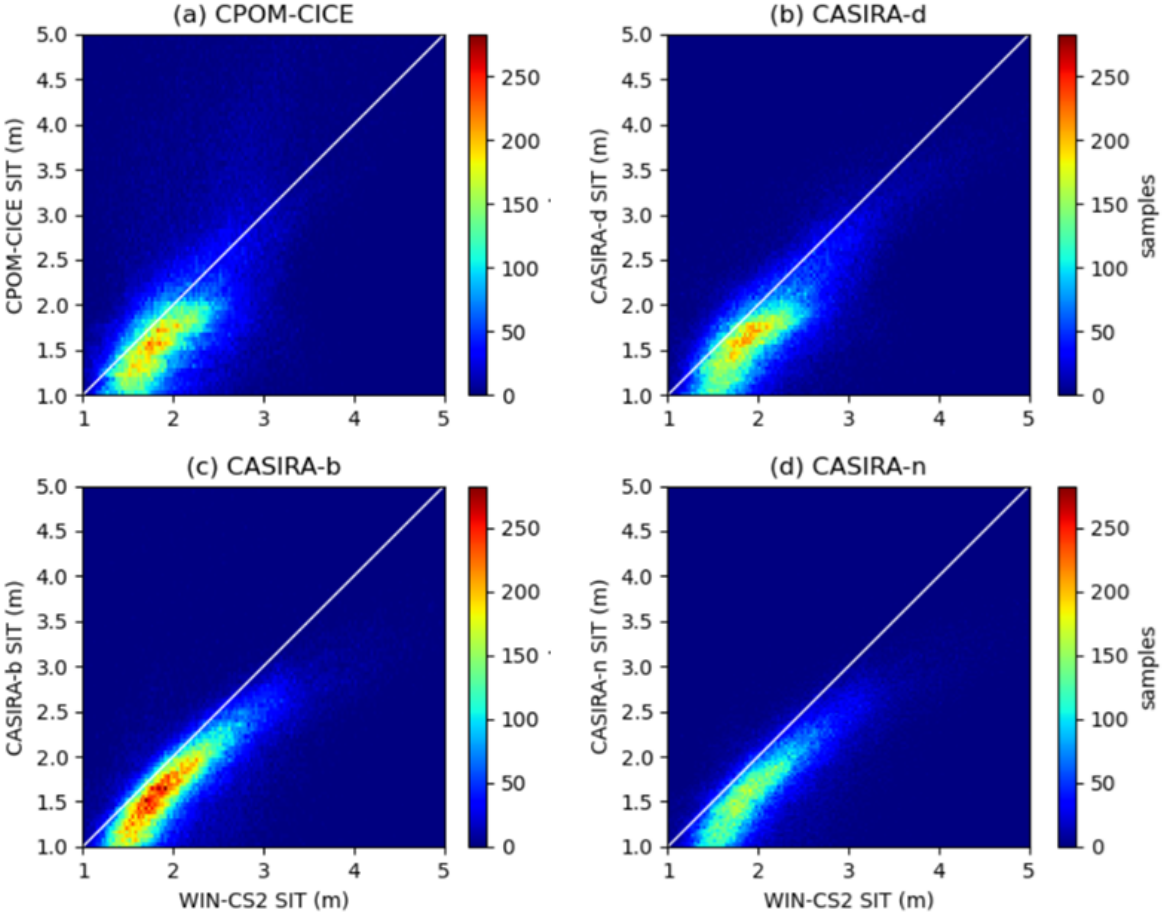

Figure 3. Density plots showing samples of coincident WIN-CS2 SIT for ensemble mean CPOM-CICE, CASIRA-d, CASIRA-b and CASIRA-n between 2010 and 2020, using monthly averages averaged across ensemble members.

that CASIRA-n and CASIRA-b perform better than CASIRA-d for OIB data, which is only available during March or April, when both WIN-CS2 and AYR-CS2 are available and measure comparable SIT values in the Arctic. This shows that the addition of summer observations for assimilation provides additional value for even late winter SIT estimates, showing that improved initialisation of SIT at the end of summer can improve SIT estimates six months later at the end of the freeze up season. This is further confirmed in the validation against BGEP ULS A, B and D data in March and April (Figure 2b), where CASIRA-n performs best against the measurements from the BGEP ULS. CASIRA-n also performs best in all three metrics for WIN-CS2, though CASIRA-b performs worse than CASIRA-d, so the difference in SIC product assimilation choice also seems to play a role. This is also seen in the difference in SIT trends in the different CASIRA reanalyses at the BGEP locations.

https://doi.org/10.5194/egusphere-2026-742
Preprint. Discussion started: 23 February 2026

3.2 Sea Ice Extent

We first investigate the long term record of SIE in the reanalyses in Figure 4. We see that in March and December the SIE in CASIRA-b, CASIRA-n and CASIRA-d are similar, with lower extents than the control run, but not so low as the reference observations. As CASIRA-n and CASIRA-d both assimilate the same SIC observations, their SIE is almost identical. In September CPOM-CICE, the reanalyses and observations are in strong agreement. CPOM-CICE September SIE is marginally lower before 2007 than the reanalyses and observations, note that this is one of the earliest significant years of September sea ice loss (Giles et al., 2008).

However, in June, there is strong disagreement between CASIRA-b and CASIRA-n. This disagreement also points to how differently the SIC observations treat melt ponds in the ice pack, with Bootstrap attempting to synthetically increase SIC more due to melt ponds. This leads to a higher SIE in the observations, and thus in the reanalysis from the SIC assimilation. However, CASIRA-b, CASIRA-n, CASIRA-d and observations do agree that there is a decreasing trend in the SIE in June, whereas CPOM-CICE shows almost no trend. Before 2000 CASIRA-b and the Bootstrap SIC observations are similar to CPOM-CICE. After 2000, however, CASIRA-b and Bootstrap SIC begin to decrease substantially, which is not the case in CPOM-CICE. The reanalyses appear to be able to better capture the increased sea ice melt shown by observations in June, though they disagree on the overall SIE. Overall, the reanalyses are better able to capture the observed trend throughout the year, and strongly agree on the SIE outside of the early summer period.

In March and December the SIEs in CASIRA-b and CASIRA-n are virtually identical, and the differences are only slightly larger in June and September. This is because NASA Team and Bootstrap generally have strong agreement in terms of extent and concentration in winter, but not so much in summer (Ivanova et al., 2015), with important differences occurring at the ice edge. We see that the assimilation is highly effective in moving the SIE estimates closer to Bootstrap observations in both reanalyses, particularly in September. We also see that both reanalyses follow the trends much closer in the observed extent than the CPOM-CICE model does. Between 1981 and 2000, SIEs in June were similar for Bootstrap, CPOM-CICE and both reanalyses. However since 2000 the June SIE in Bootstrap and the reanalyses are lower than CPOM-CICE, showing that the increasing June ice melt seen in the observations has been reproduced in the reanalyses. Note that this occurs around the same time as SIE in September began to decrease a lot. This indicates that summer sea ice melt in the peripheral seas of the Arctic has become more intense, earlier in the year than the CPOM-CICE model simulates. Gernerally, September SIE is slightly lower in CPOM-CICE, while in June SIE in CPOM-CICE is much higher, indicating a mismatch in the magnitude of the melting season at different times.

One of the main drivers for producing a reanalysis is to study and improve our understanding of climate trends over a long term period. For our reanalyses this is not perfect because there can be substantial impact of the assimilation of CS2 products in 2010 on the thickness of the sea ice - which is particularly the case for the CASIRA-b reanalysis. However concentration is

https://doi.org/10.5194/egusphere-2026-742
Preprint. Discussion started: 23 February 2026

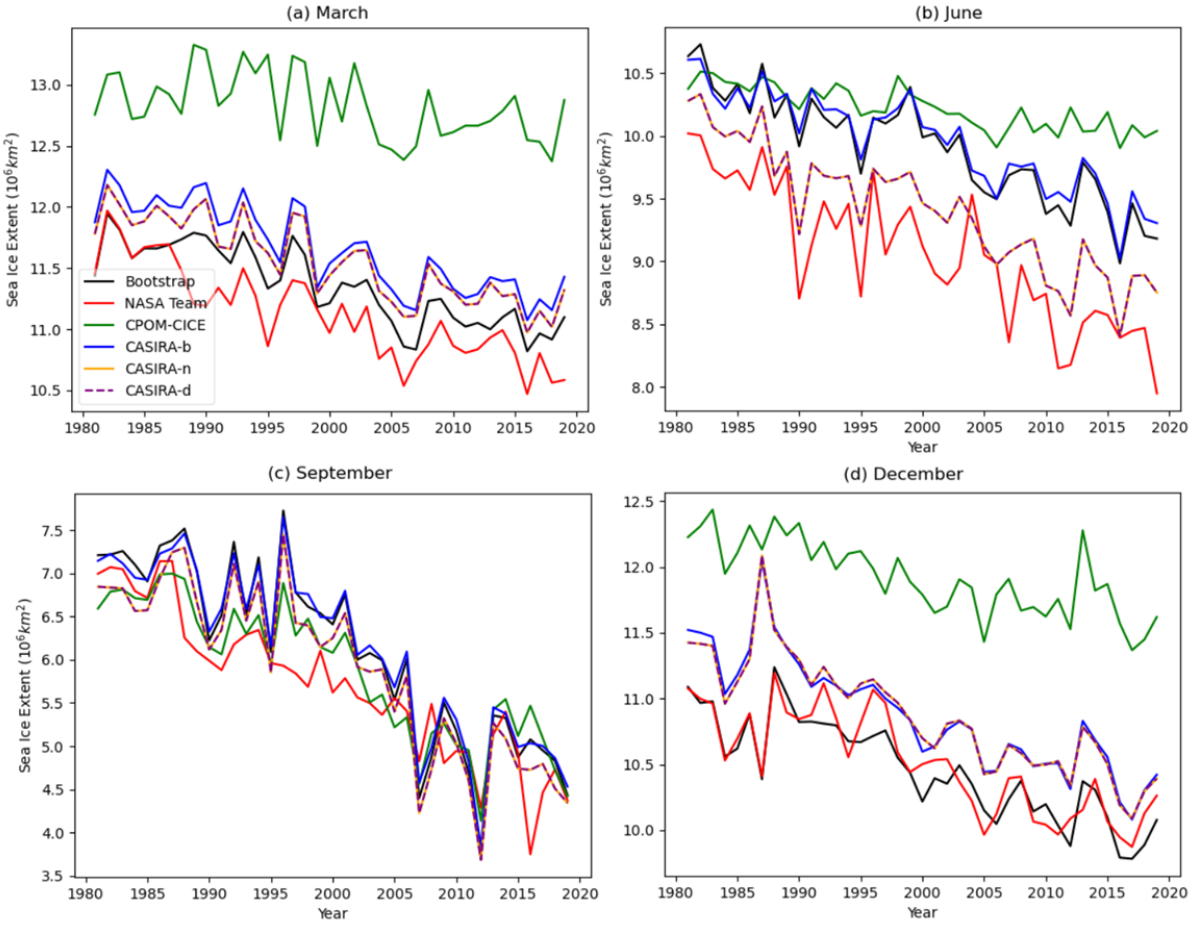

Figure 4. Monthly mean SIE averaged across ensemble members between 1981 and 2019 in the control CPOM-CICE model, ensemble means of CASIRA-b, CASIRA-n and CASIRA-d, and from the Bootstrap and NASA Team observations in March, June, September and December.

https://doi.org/10.5194/egusphere-2026-742
Preprint. Discussion started: 23 February 2026

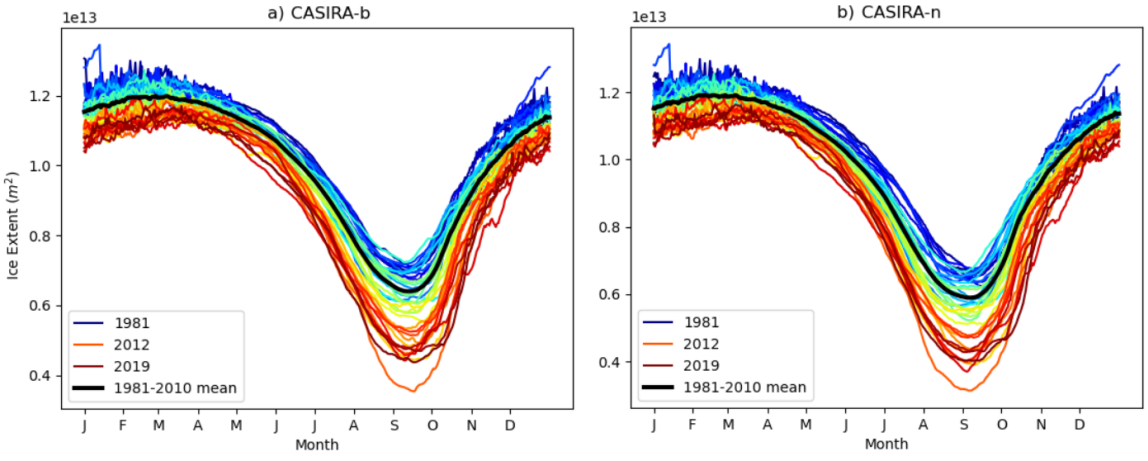

Figure 5. Monthly mean Arctic SIE averaged across ensemble members in CASIRA-b and CASIRA-n between 1981 and 2019, with climatological mean between 1981 and 2010 shown in bold.

assimilated almost consistently over the whole time period of the reanalyses and additionally assimilating SIT has limited (if any) effect on the modelled SIE in our system (Williams et al., 2023). Therefore we believe it is still valid to look at trends in the SIE over the whole reanalysis period, and compare these with trends from the control model and other observations. In Figure 5 we show the CASIRA-b and CASIRA-n ensemble mean SIE for each year from 1981-2019, and include the climatological mean for the period 1981-2010. In general the extents and their trends are very comparable, with very few differences. There are two cases in which a larger change in SIE is visible. In 1981 the larger change occurs because it is the second assimilation time step, and the differences between the model and the observations is still substantial. The second occurs in 1988 and is a result of a gap in the SIC observations between 3rd December 1987 and 13th January 1988. The size of these changes shows a significant difference in winter sea ice growth between the model with and without constraints from SIC observations, which appear to be severely overestimated in the model. As we know, the past decade has clearly seen SIEs well below the 1981-2010 climatological mean, and both reanalyses follow this trend. The minimum SIE occurs in 2012, and in 2016 the SIE was lowest between May and July and in the early freeze-up period between October and November.

3.3 Sea Ice Volume

To understand how the sea ice cover evolves more completely over the satellite era we need to look at the estimates of the SIV and how it is changing, which depends not only on the concentration but also the thickness. In Figure 6 we show monthly mean SIV for the same months as Figure 4. Before 2010 as CASIRA-n and CASIRA-d assimilate only the same SIC observations with no SIT observations, they show almost identical SIV estimates. We see that monthly mean SIV is higher between 1982 and

https://doi.org/10.5194/egusphere-2026-742
Preprint. Discussion started: 23 February 2026

2010 in CASIRA-b for all months when compared to both CPOM-CICE and PIOMAS, and much higher in March, September and December. This is an because correlations between SIC and SIT are positive on average when assimilating SIC when using Bootstrap observations in this system, which causes an increase in SIT and thus SIV. CASIRA-b SIV changes substantially in 2010, when SIT assimilation begins. This shows substantial mismatch between SIT and SIV in CASIRA-b and observations in 2010, and likely in the pre-2010 period as well. Conversely CASIRA-n and CASIRA-d SIT and SIV remain consistent pre and post 2010, so we believe there is some value in evaluating the SIT and SIV trends in these reanalyses.

CASIRA-n is strikingly similar to PIOMAS in March, September and December, and does not have the large increment in SIV when SIT assimilation begins in 2010. CASIRA-n is less comparable to PIOMAS in June, showing lower SIV during this month. The close agreement between PIOMAS and CASIRA-n is noteworthy, despite PIOMAS assimilating sea surface temperatures in ice-free grid cells and operating within a coupled ice–ocean model. It may be that sea surface temperature assimilation is more effective during the melting season, which is why PIOMAS and CASIRA-n differ in June, or that there are some differences in the sea ice model physics between PIOMAS and CPOM-CICE which lead to differences in summer. Systematic uncertainties in the CS2 SIT are also highest during this month, which could also contribute to these differences. Perhaps a superposition of these two differences cause the similarities during the growth season and the differences during the melting season. The choice of which SIC observational dataset you assimilate is very important for the reanalysis estimates of SIV.

As with SIE, we show the annual evolution of SIV and its 1981-2010 climatological mean in the reanalyses in Figure 7. There is a clear downward trend in SIV estimates in all reanalyses. In CASIRA-b there appear to be three distinct groupings. Between 1981 and 2006 ice volume is relatively high, with a few years of lower SIV in the 80s. Between 2007 and 2009 ice volume is lower than in the previous group. 2010 is also part of this group but only until September, as in October the first thickness observations are assimilated. The final group includes 2010 and subsequent years which all have much lower ice volumes than the 1981-2010 climatological mean. These are negative analysis increments from the data assimilation, showing that assimilating Bootstrap concentration alone (in the summer months) anomalously enhances ice thickness and volume. In CASIRA-n, the ice volumes are lower than in CASIRA-b, and the groupings are less clear, where there is clearly consistency in both ice concentration and thickness between the period before and after ice thickness assimilation begins. The climatological mean of 1981-2010 is between 0.6×10^{13} m^3 and 0.9×10^{13} m^3 greater in CASIRA-b than CASIRA-n, a huge difference. In CASIRA-n, winter ice volumes never exceed 3×10^{13} m^3, whereas in CASIRA-b, many winters during the 1980s reach or surpass this level.

When looking at the overall trends in these seasons, as shown in Table 3, we find that CPOM-CICE and PIOMAS are highly matched in trends, slightly different than CASIRA-n and much different to CASIRA-b. We already saw in Figure 6 that there are substantial shifts in CASIRA-b SIV and SIT when we begin to assimilate SIT, so CASIRA-b estimates of SIT and SIV in 2010 are inconsistent with those seen in observations, therefore we do not believe the trend estimates in CASIRA-b to be reliable. The trends in SIV are comparable between CPOM-CICE, PIOMAS and CASIRA-n. CASIRA-n is closely matched to

https://doi.org/10.5194/egusphere-2026-742
Preprint. Discussion started: 23 February 2026

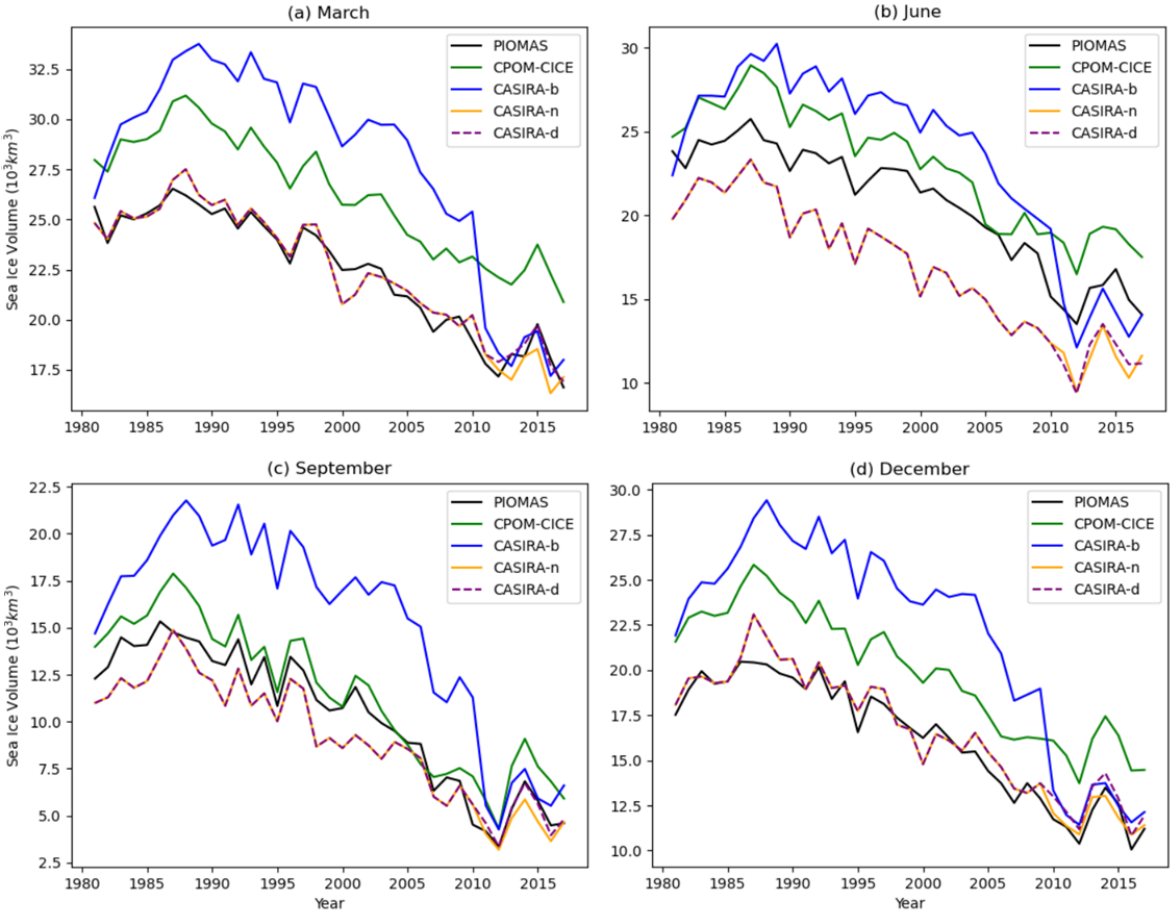

Figure 6. Ensemble monthly mean SIV between 1981 and 2019 in March, June, September and December for CPOM-CICE, CASIRA-b, CASIRA-n, CASIRA-d and the PIOMAS reanalysis.

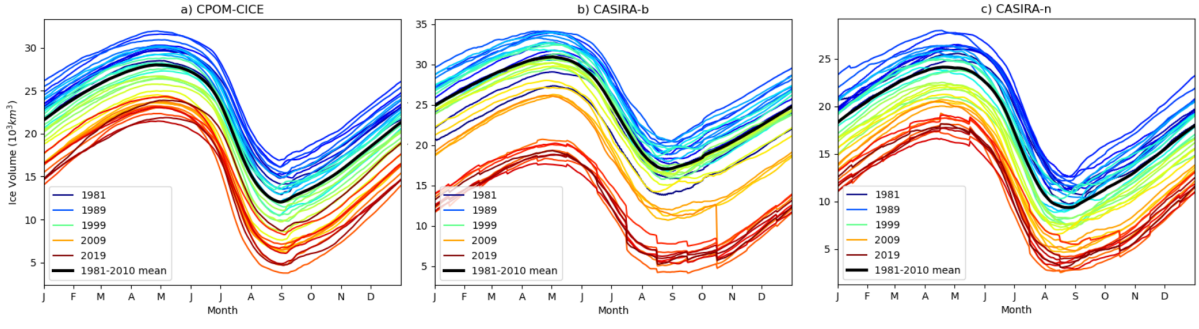

Figure 7. Ensemble mean monthly Arctic SIV in CASIRA-b and CASIRA-n between 1981 and 2019, with the climatological mean between 1981 and 2010 shown in bold. In the past decade SIE has been significantly below the 1981-2010 mean.

https://doi.org/10.5194/egusphere-2026-742
Preprint. Discussion started: 23 February 2026

Table 3. Monthly mean interannual sea ice volume trends in km^3 / month for March, June, September and December in CPOM-CICE, CASIRA-b, CASIRA-n and PIOMAS between 1981 and 2020.

Model	March	June	September	December
CPOM-CICE	-246	-304	-322	-295
CASIRA-b	-308	-371	-346	-381
CASIRA-n	-247	-345	-262	-281
CASIRA-d	-244	-343	-257	-272
PIOMAS	-249	-306	-312	-279

PIOMAS and CPOM-CICE in March and December, but the September SIV trend is lower, while the June trend is higher. This may indicate an increase in intensity of the early melt season in many regions of the Arctic, or large uncertainty in estimates of the melting season intensity coming from the observations. All experiments agree that SIV in the 2010+ period is well below the 1981-2010 climatological mean. We will next look at how the SIT compares between the CPOM-CICE model, CASIRA, PIOMAS, WIN-CS2 and AYR-CS2.

3.4 Sea Ice Thickness

We have found that in many cases there are comparable SIVs between our reanalyses and CPOM-CICE, despite very differing estimates of SIE. This means that the SIT in the Arctic must be distributed in different ways between our control and reanalyses. Here we investigate the spatial distribution of the SIT in the Arctic in our reanalyses and compare it with those from CPOM-CICE, PIOMAS and the AYR-CS2 observations. In Figure 8 we show the March and September SIT climatologies between 1981 and 2010, and then between 2011 and 2019. The AYR-CS2 product has a particular spatial distribution, with some thicker ice directly over the pole, which has not been seen in previous Arctic sea ice reanalyses, models or observations. This is an effect from the snow model accumulation scheme used in the product, which shows some of the thickest snow depths north of the Fram Strait. The SIT in AYR-CS2 also generally appears to exhibit less thick ice packed against the CAA, commonly seen elsewhere. The CPOM-CICE model has too much thick ice packed against the CAA and Northern Greenland (particularly in September), and is too thin in the rest of the Arctic in comparison with AYR-CS2, PIOMAS and CASIRA in both September and March and in both 1981-2010 and 2010-2020. It appears that there is a tendency in the model to push too much ice into the central pack against the CAA, and additionally that the thickest ice near the CAA is too resistant to the summer melting season - it does not thin as much as the observations show.

Between 1981 and 2010, PIOMAS compares best with CASIRA-n, while CASIRA-b and CPOM-CICE both have substantially thick ice packed up against the CAA for both March and September. For the 2010-2020 climatologies however, CASIRA-b is much more comparable to PIOMAS as the assimilation of AYR-CS2 begins. This is particularly true in September. In March

https://doi.org/10.5194/egusphere-2026-742
Preprint. Discussion started: 23 February 2026

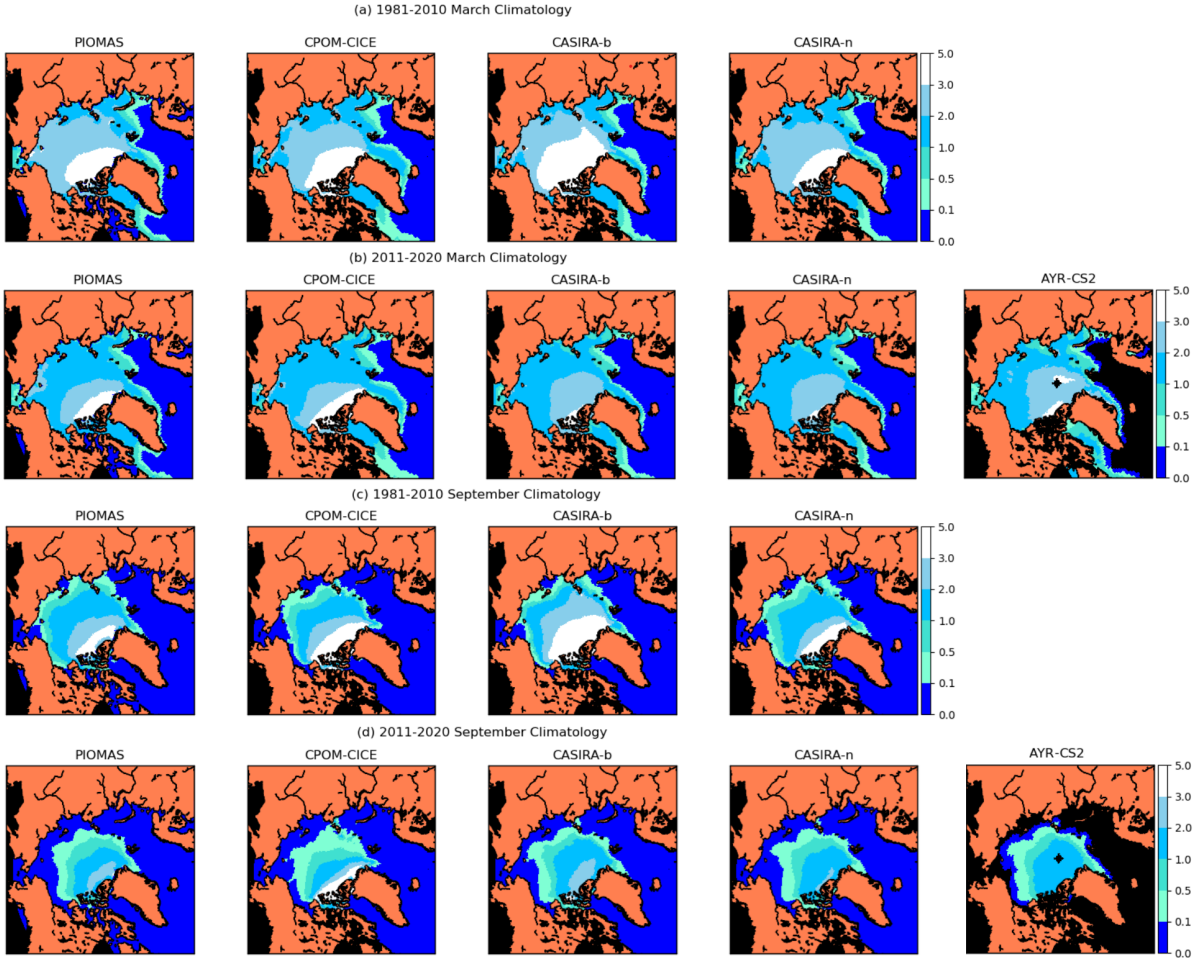

Figure 8. Monthly and ensemble mean SIT in March and September for PIOMAS, CPOM-CICE, CASIRA-b, CASIRA-n, and AYR-CS2 (when available) for (a) 1981-2010 March (b) 2011-2020 March (c) 1981-2010 September (d) 2010-2020 September.

CASIRA-b and CASIRA-n show very few areas of sea ice thicker than 3 m, similar to the assimilated AYR-CS2. In September 2010-2020, CPOM-CICE still shows an area of ice thicker than 3 m, which does not appear in the other products.

In our reanalyses we see substantial differences, in models, reanalyses and observations in the distribution of the SIT across the Arctic, particularly in the period between 2010-2020, where AYR-CS2, CASIRA and even PIOMAS to a certain degree, show an almost complete disappearance of the thickest ice packed against the CAA, but with thicker ice extending further outwards from the CAA. This shows a possible change in the distribution shape of SIT in the Arctic from the early satellite period to the most recent decade - this demonstrates the regime shift in SIT shown in Sumata et al. (2023).

https://doi.org/10.5194/egusphere-2026-742
Preprint. Discussion started: 23 February 2026

3.5 Comparison of CASIRA-n with CPOM-CICE in the 2010-2020 period

The 2010–2020 decade in our reanalysis is the most informative period, as this is when we (a) assimilate both SIE and SIT and (b) have the most observations available for validation. We have seen already that our CASIRA-n reanalysis compares well with PIOMAS and independent observations, and so in this section we choose to focus solely on this reanalysis for the 2010+ period and compare it with our free model, to deepen our understanding of the model, and in particular attempt to identify problems and potentially missing physics in the model.

CPOM-CICE shows a positive bias in SIE over most of the year (Figure 9). It persists at the same magnitude between November and May during the growth season. The positive bias increases over June and July, but reduces sharply in August, and then further decreases, leading to zero bias in September and October. The bias then re-emerges quickly in November. The persistent bias in the freeze-up season in CPOM-CICE is primarily indicative of a known cold bias in the atmospheric reanalysis, which is present in the NCEP-2 reanalysis in the Arctic of up to 5 degrees K in the seas surrounding the Arctic (Batrak and Müller, 2019). The sudden increase in bias between October and November is caused partially by this rapid freeze up of sea ice in the marginal seas, but there are also further factors at play: leads in the sea ice cover could be more prevalent than expected, or wider than expected at the end of summer, which if not represented in the model would lead to faster lead close-up than in reality. However the main cause for this increase is that the SIE increases more quickly in the model due to heat being lost more rapidly in the ocean, or that the ocean is colder.

The SIE positive bias is stable over the freeze-up season in CPOM-CICE, however the SIT and SIV biases grow over winter (Figure 10). This suggests a snow depth over the sea ice which is too low, increasing conductive cooling through the snow and ice, leading to excessive ice growth in the ice pack and causing the winter SIT bias growth. Snow depth remains difficult to verify in the Arctic due to limited reliable observations, though ongoing work and the upcoming ESA CRISTAL mission should improve understanding of its distribution (Landy et al., 2024). Leads refreezing may also play a role in the error in the early freeze up season, if they are refreezing too quickly due to an underestimation of their scale or quantity. There may also be missing processes in the model that enhance negative feedbacks on SIT growth in winter.

In the May-July period, CASIRA-n exhibits larger reductions in both sea ice extent and volume than CPOM-CICE (Figures 9 and 10). Meanwhile August and September show an inverse relationship, with melting higher in CPOM-CICE than CASIRA-n. This leads to agreement in SIE between CASIRA-n and CPOM-CICE in September, while also reducing the CPOM-CICE positive SIV bias to its yearly minimum. The thicker ice in CPOM-CICE will be more resistant to breakup and melting. This is clearly seen in Figures 9 and 11, where we see that CASIRA-n shows a greater MIZ area than CPOM-CICE in May and June. Another source of this spring melting error may be that melt pond rates at ice on the ice edge are underestimated, and if a floe size distribution parametrisation were included, it may also account for dynamical and thermodynamical processes on the

https://doi.org/10.5194/egusphere-2026-742
Preprint. Discussion started: 23 February 2026

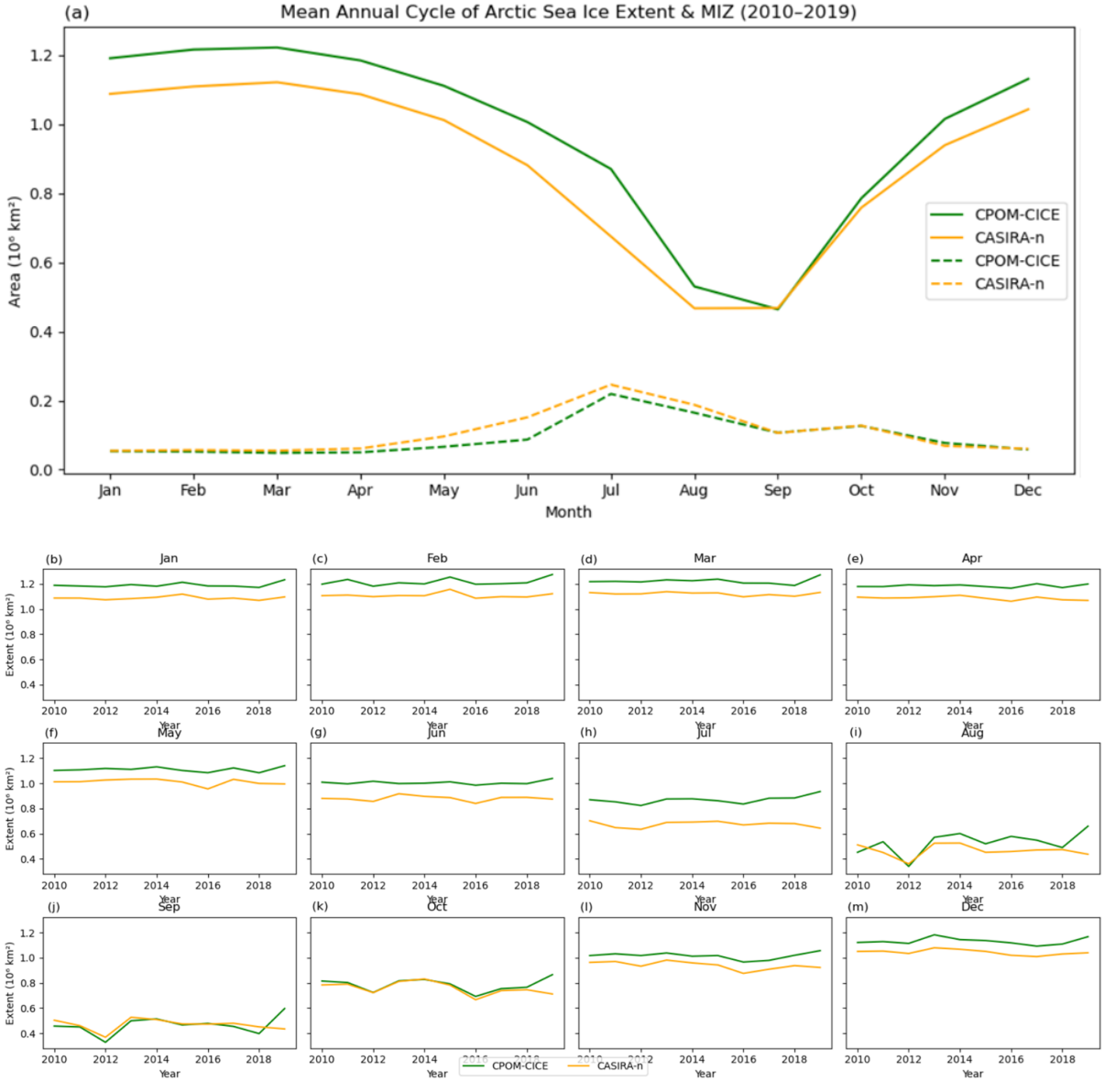

Figure 9. Top: Monthly climatology of ensemble mean CPOM-CICE and CASIRA-n SIE (solid lines) and MIZ (dashed lines) area over the 2010-2020 period. Bottom: Time series of monthly mean SIE in each month over the 2010-2020 period

https://doi.org/10.5194/egusphere-2026-742
Preprint. Discussion started: 23 February 2026

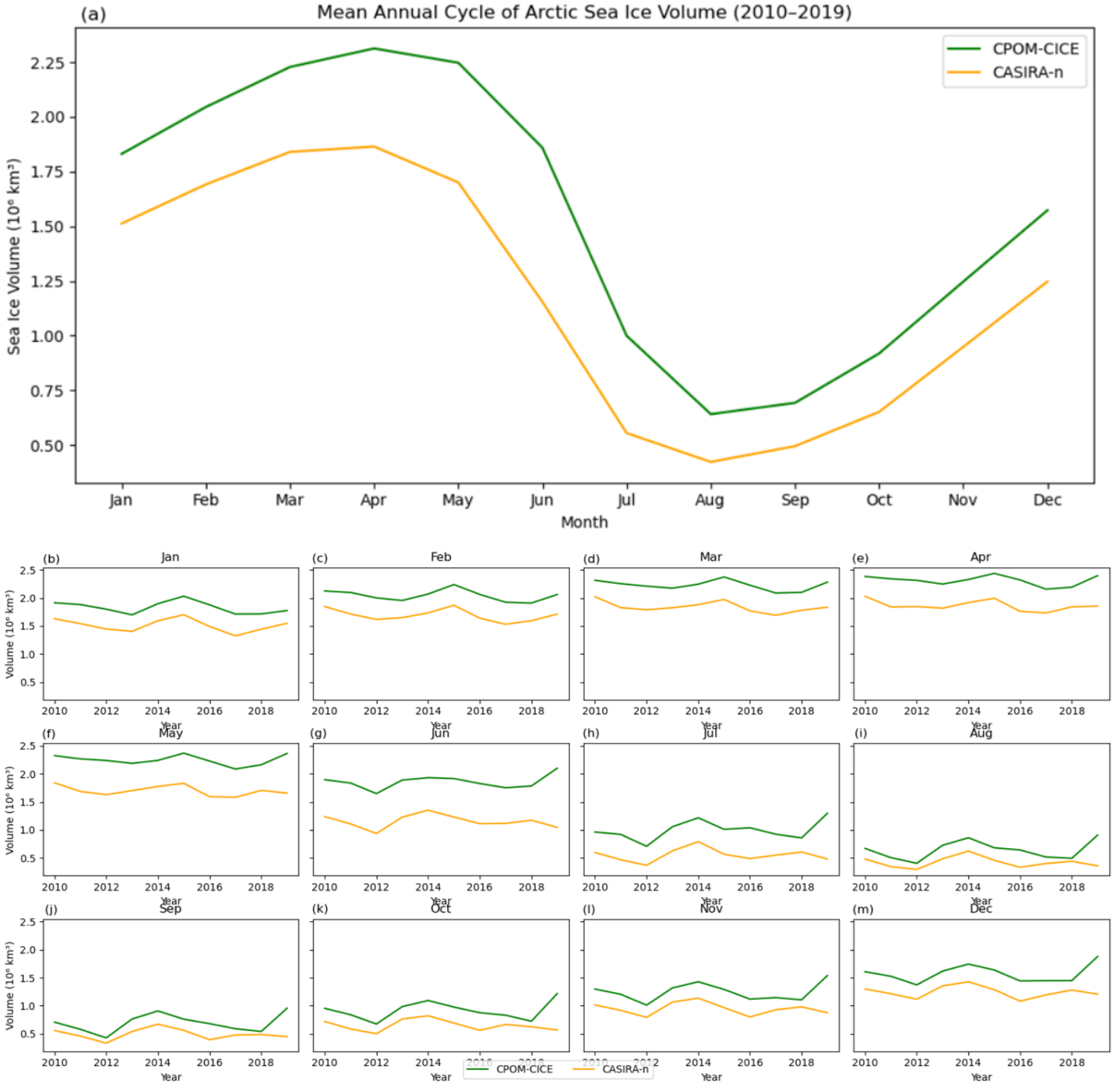

Figure 10. Top: Monthly climatology of CPOM-CICE and CASIRA-n SIV over the 2010-2020 period averaged across ensemble members. Bottom: Time series of monthly mean SIV in each month over the 2010-2020 period averaged across ensemble members.

https://doi.org/10.5194/egusphere-2026-742
Preprint. Discussion started: 23 February 2026

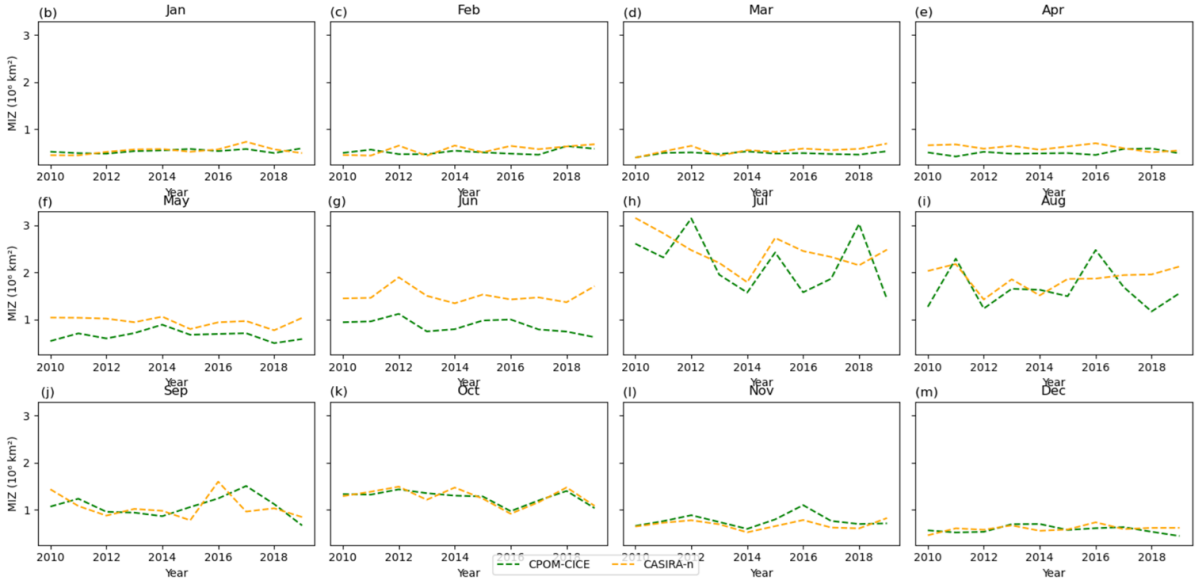

Figure 11. Time series of monthly mean MIZ area averaged across ensemble members in CPOM-CICE and CASIRA-n for each month over the 2010-2020 period.

sea ice edge more accurately in the model and produce a more physically robust MIZ (Bateson et al., 2020; Frew et al., 2025). If these sea ice edge processes are underestimated they would account for the negative MIZ bias. Additionally, AYR-CS2 estimates of SIT are most uncertain during June and July due to the poorly understood effects of melt pond loading on sea ice after snowmelt, which could introduce systematic biases in SIT and the timing of thinning.

The increased August–September melt in CPOM-CICE likely reflects a compensation for earlier underestimation of melt. Thicker ice will take longer to melt due to thermodynamic processes. This is also shown in the thickness of the ice leftover in September - in CPOM-CICE the remaining ice is much thicker than in CASIRA-n in most of the ice pack, aside from a region around the North Pole. It is particularly much thicker around the CAA. Additionally, this could be linked to too-high solar absorption in the model for thinner ice, which may be linked to an incorrect representation of albedo feedbacks for thin and thick ice. Figure 12 demonstrates too-thin sea ice present in CPOM-CICE in the region around the North Pole. As we too-thick sea ice in the CAA, but too-thin around the north pole peaking in September, there may be a mismatch in the sea ice transport, possibly connected to the rheology allowing too much ridging. Too much ice may be advected into the CAA, and not enough through the North Pole, some of which may later be advected out into the Fram Strait.

We investigate the changes in the SITD across the Arctic in Figure 13. For most of the year CPOM-CICE SIT distribution peaks at around 2 metres, however we find extreme seasonal transitions, with much less thin ice in March, June and December than seen in September. In September the CPOM-CICE sea ice cover is dominated by thin ice. The ice cover between 1 and 3

https://doi.org/10.5194/egusphere-2026-742
Preprint. Discussion started: 23 February 2026

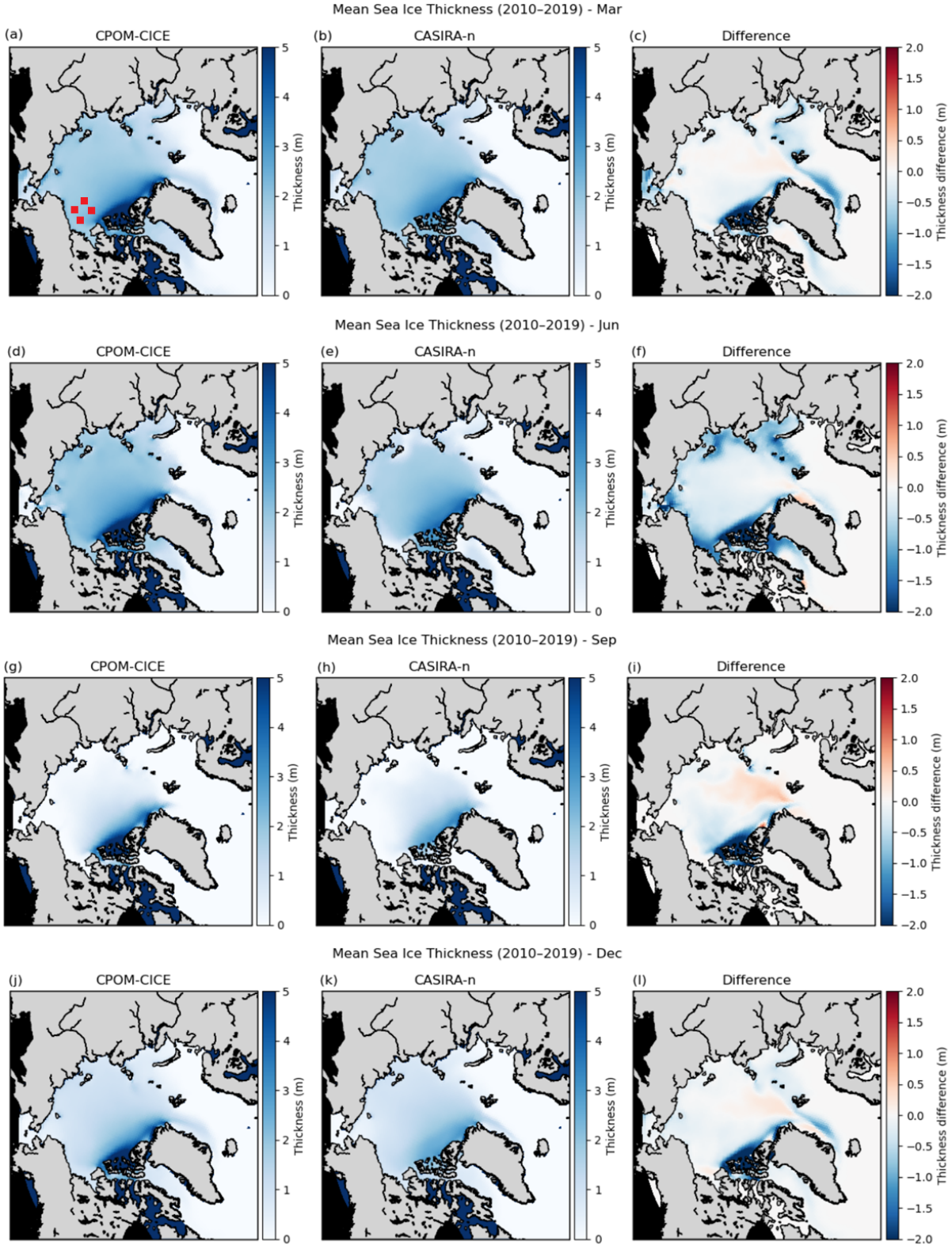

Figure 12. March, June, September and December mean sea ice thickness over the 2010-2020 period in CPOM-CICE and CASIRA-n and the difference between the two (CASIRA-n - CPOM-CICE). The locations of the BGEP ULS moorings are shown as red squares in panel (a).

https://doi.org/10.5194/egusphere-2026-742
Preprint. Discussion started: 23 February 2026

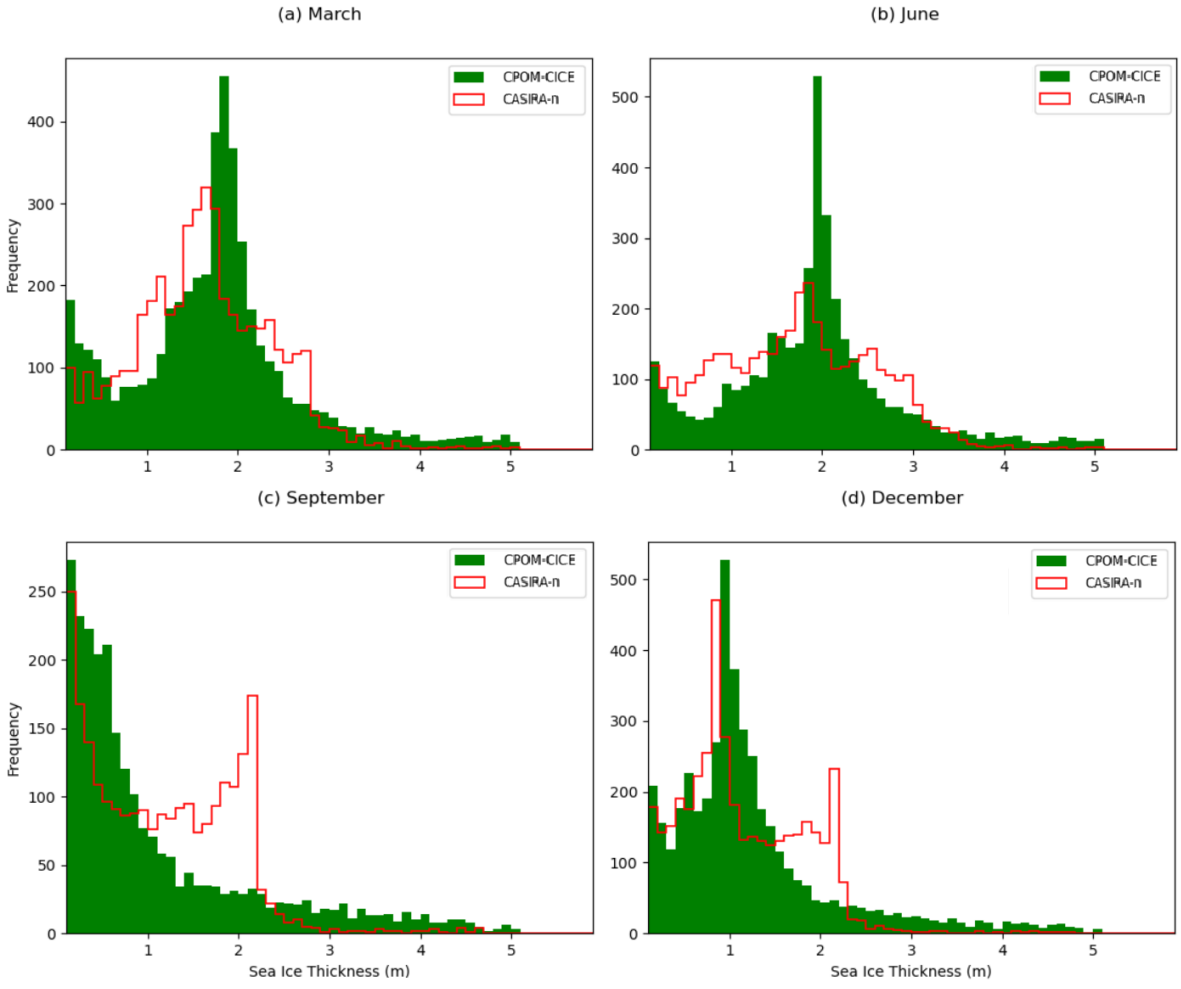

Figure 13. Histogram showing monthly mean pan-Arctic SIT in each grid cell in March, June, September and December between 2011 and 2020 for CPOM-CICE, and CASIRA-n, between 2011 and 2019.

metres has been melted away in CPOM-CICE, leaving a large area of thin ice, and the too-thick ice pack in the CAA. Between September and December the ice has thickened rapidly in CPOM-CICE, and a peak around 1-2 metres is established quickly. In CASIRA-n we see a much broader distribution of the ice thickness, with much less ice thicker than 3 metres in CASIRA-n.

4 Discussion

Comparison with PIOMAS revealed large differences in SIV estimates. When NASA Team observations were assimilated (e.g. CASIRA-n), the volume estimates were similar to PIOMAS estimates in the freeze-up season. However there were lower

https://doi.org/10.5194/egusphere-2026-742
Preprint. Discussion started: 23 February 2026

estimates of volume in the melting season (June and September) in comparison to PIOMAS. These differences in the melting season were smaller after 2005. As PIOMAS also assimilates NASA Team data we expect the differences in volume should be small, so the differences in summer are quite stark. When looking at the mean ice thickness, there are big differences in the distribution of the SIT across the Arctic, particularly in the Central Arctic and the CAA. PIOMAS has much thinner ice in the CAA than the CPOM-CICE model and CASIRA-b, but a larger region of sea ice over 1.4 m thick covering much of the central Arctic Ocean even in September. CASIRA-n shows a more similar distribution to PIOMAS but there is strong disagreement between PIOMAS and CASIRA-n in the central Arctic. The consensus within our sea ice reanalyses seems to be thicker ice in the Central Arctic than in sea ice models, which evaluates well against independent observations (particularly for CASIRA-n). A notable difference between trends in our reanalyses and those from PIOMAS is that the September trend in our reanalyses is much smaller, but the trend in June is greater. Trends in SIV for CASIRA-n are still well matched to PIOMAS and CPOM-CICE.

CASIRA-n shows substantially lower RMSE across all three validation datasets compared to CPOM-CICE. It also shows improved agreement with BGEP ULS validation data from pre-2010. The areas of strongest improvement are in the central Arctic, Beaufort Sea and the region around the North Pole. These areas are identified in Chevallier et al. (2017) as regions where current reanalyses of Arctic sea ice are deficient, indicating that CASIRA-n reduces known regional biases. There is a need for further work in quantifying the errors of sea ice observations, as many sea ice observation datasets do not provide fully quantified uncertainties, which are important for data assimilation.

Over 2010–2020, CPOM-CICE exhibits a persistent positive sea ice extent bias during the freeze-up season and a growing winter bias in sea ice thickness and volume relative to CASIRA-n, linked to cold atmospheric forcing, underestimated snow depth, and overly rapid ocean heat loss. Melt season behaviour differs, with CASIRA-n showing stronger spring–early summer retreat, while CPOM-CICE compensates with enhanced late-summer melt, leading to agreement in September extent but maintaining a positive thickness bias. CPOM-CICE also underestimates MIZ area in spring, suggesting missing or weakly represented sea ice edge processes such as melt pond evolution and floe size dynamics. Spatial and thickness distribution analyses further indicate excessive ice thickening and redistribution toward the Canadian Arctic Archipelago and a narrower thickness distribution in CPOM-CICE, pointing to potential biases in sea-ice transport and rheology. Overall, CPOM-CICE overestimates early winter growth, underestimates spring-early summer melt and overestimates late summer melt - exhibiting a too-strong seasonal cycle.

Comparisons of SIC, SIE, SIT, and SIV between CASIRA-n, CPOM-CICE, and PIOMAS reveal the largest disagreements during the May–August melting season, particularly in the early melt period. In contrast, all systems show strong agreement in September for both extent and volume. Trends are generally consistent across CASIRA-n, PIOMAS, and CPOM-CICE, except in June, where CASIRA-n exhibits a stronger decreasing trend in volume. Overall, CASIRA-n demonstrates the most consistent trends in SIC, SIT, and SIV across the satellite era. Assimilation of NASA Team SIC effectively constrained SIT

https://doi.org/10.5194/egusphere-2026-742
Preprint. Discussion started: 23 February 2026

prior to 2010, with only minor adjustments required when SIT assimilation began.

In the pre-2010 period, the reanalyses exhibit larger spread and variability in SIV, reflecting sparser observations and the absence of SIT assimilation, which limits constraints on the sea ice mass budget. From 2010 onward, when SIT assimilation begins, SIV estimates partially converge and agreement with PIOMAS improves, with the reanalyses also outperforming the control run when evaluated against independent datasets. Winter SIV trends are consistent across CASIRA-n, PIOMAS, and CPOM-CICE, whereas spring and summer trends diverge, with CASIRA-n showing stronger declines in June and PIOMAS and CPOM-CICE exhibiting larger decreases in September.

5 Conclusions

We have produced three new Arctic sea ice reanalyses (CASIRA-b, -n and -d) over the satellite era, incorporating recently available year-round SIT observations. The inclusion of these observations, not previously available, improves estimates of SIT and SIV during the melt season. CASIRA-n shows the best skill, and compares well with both the CPOM-CICE model and PIOMAS, with the assimilation of year-round SIT shown to improve SIT estimates at the end of the growth season (March–April) relative to using winter SIT alone. This highlights the additional benefit of end-of-summer SIT initialisation for winter sea ice estimates.

A comparison of CASIRA-n with CPOM-CICE highlights model deficiencies and identifies priorities for future sea ice modelling. Winter sea ice growth is excessive in CPOM-CICE, particularly at the ice edge, likely influenced by cold-biased atmospheric forcing, with too rapid ocean cooling and representation of leads also contributing. Within the ice pack, positive SIT biases are likely caused by underestimation of snow depth, rapid re-freezing of leads, or other processes that act as negative feedbacks to winter SIT growth. Spring ice-edge errors may be linked to the absence of a floe size distribution parameterisation, potential melt pond inaccuracies, and excessive thickening during winter. Delays and magnitude errors in the melting season stem from excessive winter growth in the central ice pack and under-represented melting feedbacks (e.g., albedo, melt ponds). Validation shows that CASIRA-n has substantially reduced errors in SIC and SIT, better constrains winter growth, improves MIZ representation in spring, and produces a more realistic spatial distribution of SIT. These results highlight a significant mismatch between model and reanalysis in the seasonal cycle and emphasize the need for further work to reduce uncertainty during seasonal transitions.

Finally, our analysis demonstrates the importance of assimilating SIT alongside SIC. Incorporating year-round SIT observations further reduces uncertainties in SIT and SIV, improving estimates of Arctic sea ice state and trends. Assimilation of summer SIT is particularly promising for future reanalyses and prediction studies, providing pathways to improve sea ice modelling and better constrain Arctic sea ice variability over the satellite era.

https://doi.org/10.5194/egusphere-2026-742
Preprint. Discussion started: 23 February 2026

Code and data availability. CICE v5.1.2 is available from: https://github.com/CICE-Consortium/CICE-svn-trunk/tree/cice-5.1.2. PDAF v2.0 is available for download here: https://pdaf.awi.de/. Operation IceBridge Level 1 quick-look data is found here: https://nsidc.org/data/nsidc-0708/versions/1. Operation IceBridge Level 4 data is found here: https://nsidc.org/data/idcsi4/versions/1. Bootstrap sea ice concentration data is available from: https://nsidc.org/data/nsidc-0079/versions/4. NASA Team sea ice concentration is available from: https://climatedataguide.ucar.edu/climate-data/sea-ice-concentration-data-nasa-goddard-and-nsidc-based-nasa-team-algorithm. WIN-CS2 SIT is available from: https://www.cpom.ucl.ac.uk/eocis/seaice/download_info.php. AYR-CS2 is available from: https://data.bas.ac.uk/full-record.php?id=GB/NERC/BAS/PDC/01613. The BGEP data were collected and made available at https://www2.whoi.edu/site/beaufortgyre/ by the Beaufort Gyre Exploration Program based at the Woods Hole Oceanographic Institution in collaboration with researchers from Fisheries and Oceans Canada at the Institute of Ocean Sciences. During the revision phase, the reanalysis data and scripts used in this study will be uploaded to a Research Data Archive and shared under an Open-Access license.

Author contributions. The coupled CICE–PDAF model was developed by NB with support from LN and NW. NW further developed CICE–PDAF for assimilation of sea ice observations. Observations were processed for assimilation and evaluation by NW, DS and IL. NW performed the simulations and analysis under the supervision of DF, DS, PJVL, RB and NB. NB and DS provided additional technical support. JL and GD provided technical support for use of the year-round CS2 observations. The manuscript was written by NW with contributions and feedback from all authors.

Competing interests. Daniel Feltham and David Schroeder are members of the editorial board of The Cryosphere.

Acknowledgements. We would like to thank Maria Broadridge for her technical support during this work. CICE–PDAF simulations were performed on the ARCHER2 UK national supercomputing service. This research has been supported by the Natural Environment Research Council (grant no. F4026715).

https://doi.org/10.5194/egusphere-2026-742
Preprint. Discussion started: 23 February 2026

References

Arruda, G. M. and Krutkowski, S.: Social impacts of climate change and resource development in the Arctic: Implications for Arctic governance, Journal of Enterprising Communities: People and Places in the Global Economy, 11, 277–288, 2017.

Bateson, A. W., Feltham, D. L., Schröder, D., Hosekova, L., Ridley, J. K., and Aksenov, Y.: Impact of sea ice floe size distribution on seasonal fragmentation and melt of Arctic sea ice, The Cryosphere, 14, 403–428, 2020.

Batrak, Y. and Müller, M.: On the warm bias in atmospheric reanalyses induced by the missing snow over Arctic sea-ice, Nature Communications, 10, 4170, 2019.

Beaven, S. G.: Sea ice radar backscatter modeling, measurements, and the fusion of active and passive microwave data, University of Kansas, 1995.

Bennetts, L., Bitz, C., Feltham, D., Kohout, A., and Meylan, M.: Marginal ice zone dynamics: Future research perspectives and pathways, Philosophical Transactions of the Royal Society A, 380, 20210 267, 2022.

Bitz, C. M. and Lipscomb, W. H.: An energy-conserving thermodynamic model of sea ice, Journal of Geophysical Research: Oceans, 104, 15 669–15 677, 1999.

Blockley, E. W. and Peterson, K. A.: Improving Met Office seasonal predictions of Arctic sea ice using assimilation of CryoSat-2 thickness, The Cryosphere, 12, 3419–3438, 2018.

Boutin, G., Lique, C., Ardhuin, F., Rousset, C., Talandier, C., Accensi, M., and Girard-Ardhuin, F.: Towards a coupled model to investigate wave–sea ice interactions in the Arctic marginal ice zone, The Cryosphere, 14, 709–735, 2020.

Briegleb, B. and Light, B.: A Delta-Eddington multiple scattering parameterization for solar radiation in the sea ice component of the Community Climate System Model, NCAR technical note, pp. 1–108, 2007.

Bunzel, F., Notz, D., and Pedersen, L. T.: Retrievals of Arctic sea-ice volume and its trend significantly affected by interannual snow variability, Geophysical Research Letters, 45, 11–751, 2018.

Cavalieri, D. J. and Parkinson, C. L.: Arctic sea ice variability and trends, 1979–2010, The Cryosphere, 6, 881–889, 2012.

Chevallier, M., Smith, G. C., Dupont, F., Lemieux, J.-F., Forget, G., Fujii, Y., Hernandez, F., Msadek, R., Peterson, K. A., Storto, A., et al.: Intercomparison of the Arctic sea ice cover in global ocean–sea ice reanalyses from the ORA-IP project, Climate Dynamics, 49, 1107–1136, 2017.

Comiso, J.: Bootstrap Sea Ice Concentrations from Nimbus-7 SMMR and DMSP SSM/I-SSMIS, Version 3, boulder, Colorado USA. NASA National Snow and Ice Data Center Distributed Active Archive Center, 2017.

Comiso, J. C., Cavalieri, D. J., Parkinson, C. L., and Gloersen, P.: Passive microwave algorithms for sea ice concentration: A comparison of two techniques, Remote sensing of Environment, 60, 357–384, 1997.

Dai, A., Luo, D., Song, M., and Liu, J.: Arctic amplification is caused by sea-ice loss under increasing CO2, Nature communications, 10, 1–13, 2019.

David, C., Lange, B., Krumpen, T., Schaafsma, F., van Franeker, J. A., and Flores, H.: Under-ice distribution of polar cod Boreogadus saida in the central Arctic Ocean and their association with sea-ice habitat properties, Polar Biology, 39, 981–994, 2016.

Dawson, G., Landy, J., Tsamados, M., Komarov, A. S., Howell, S., Heorton, H., and Krumpen, T.: A 10-year record of Arctic summer sea ice freeboard from CryoSat-2, Remote Sensing of Environment, 268, 112 744, 2022.

Eayrs, C., Li, X., Raphael, M. N., and Holland, D. M.: Rapid decline in Antarctic sea ice in recent years hints at future change, Nature Geoscience, 14, 460–464, 2021.

https://doi.org/10.5194/egusphere-2026-742
Preprint. Discussion started: 23 February 2026

Farrell, S. L., Kurtz, N., Connor, L. N., Elder, B. C., Leuschen, C., Markus, T., McAdoo, D. C., Panzer, B., Richter-Menge, J., and Sonntag, J. G.: A first assessment of IceBridge snow and ice thickness data over Arctic sea ice, IEEE Transactions on Geoscience and Remote Sensing, 50, 2098–2111, 2011.

Ferry, N., Masina, S., Storto, A., Haines, K., Valdivieso, M., Barnier, B., and Molines, J.-M.: Product User Manual GLOBALREANALYSISPHYS-001-004-a and b, 2011.

Fiedler, E. K., Martin, M. J., Blockley, E., Mignac, D., Fournier, N., Ridout, A., Shepherd, A., and Tilling, R.: Assimilation of sea ice thickness derived from CryoSat-2 along-track freeboard measurements into the Met Office's Forecast Ocean Assimilation Model (FOAM), The Cryosphere, 16, 61–85, 2022.

Flocco, D., Feltham, D. L., and Turner, A. K.: Incorporation of a physically based melt pond scheme into the sea ice component of a climate model, Journal of Geophysical Research: Oceans, 115, 2010.

Francis, J. A., Vavrus, S. J., and Cohen, J.: Amplified Arctic warming and mid-latitude weather: new perspectives on emerging connections, Wiley Interdisciplinary Reviews: Climate Change, 8, e474, 2017.

Frew, R. C., Bateson, A. W., Feltham, D. L., and Schröder, D.: Toward a marginal Arctic sea ice cover: changes to freezing, melting and dynamics, The Cryosphere, 19, 2115–2132, 2025.

Fritzner, S., Graversen, R., Christensen, K. H., Rostosky, P., and Wang, K.: Impact of assimilating sea ice concentration, sea ice thickness and snow depth in a coupled ocean–sea ice modelling system, The Cryosphere, 13, 491–509, 2019.

Gaspari, G. and Cohn, S. E.: Construction of correlation functions in two and three dimensions, Quarterly Journal of the Royal Meteorological Society, 125, 723–757, 1999.

Giles, K. A., Laxon, S. W., and Ridout, A. L.: Circumpolar thinning of Arctic sea ice following the 2007 record ice extent minimum, Geophysical Research Letters, 35, 2008.

Horvat, C.: Floes, the marginal ice zone and coupled wave-sea-ice feedbacks, Philosophical Transactions of the Royal Society A, 380, 20210 252, 2022.

Hunke, E., Lipscomb, W., Turner, A., Jeffery, N., and Elliott, S.: CICE: The Los Alamos sea ice model documentation and software user's manual 1568 version 5.1, Tech. rep., Los Alamos National Laboratory, 2015.

Hunt, B. R., Kostelich, E. J., and Szunyogh, I.: Efficient data assimilation for spatiotemporal chaos: A local ensemble transform Kalman filter, Physica D: Nonlinear Phenomena, 230, 112–126, 2007.

Hunter, C. M., Caswell, H., Runge, M. C., Regehr, E. V., Amstrup, S. C., and Stirling, I.: Climate change threatens polar bear populations: a stochastic demographic analysis, Ecology, 91, 2883–2897, 2010.

Ivanova, N., Johannessen, O. M., Pedersen, L. T., and Tonboe, R. T.: Retrieval of Arctic sea ice parameters by satellite passive microwave sensors: A comparison of eleven sea ice concentration algorithms, IEEE Transactions on Geoscience and Remote Sensing, 52, 7233–7246, 2014.

Ivanova, N., Pedersen, L. T., Tonboe, R., Kern, S., Heygster, G., Lavergne, T., Sørensen, A., Saldo, R., Dybkjær, G., Brucker, L., et al.: Inter-comparison and evaluation of sea ice algorithms: towards further identification of challenges and optimal approach using passive microwave observations, The Cryosphere, 9, 1797–1817, 2015.

Kanamitsu, M., Ebisuzaki, W., Woollen, J., Yang, S.-K., Hnilo, J., Fiorino, M., and Potter, G.: Ncep–doe amip-ii reanalysis (r-2), Bulletin of the American Meteorological Society, 83, 1631–1644, 2002.

Krishfield, R. and Proshutinsky, A.: BGOS ULS data processing procedure, Woods Hole Oceanographic Institution, 2006.

https://doi.org/10.5194/egusphere-2026-742
Preprint. Discussion started: 23 February 2026

Krishfield, R. A., Proshutinsky, A., Tateyama, K., Williams, W. J., Carmack, E. C., McLaughlin, F. A., and Timmermans, M.-L.: Deterioration of perennial sea ice in the Beaufort Gyre from 2003 to 2012 and its impact on the oceanic freshwater cycle, Journal of Geophysical Research: Oceans, 119, 1271–1305, 2014.

Kurtz, N., Farrell, S., Studinger, M., Galin, N., Harbeck, J., Lindsay, R., Onana, V., Panzer, B., and Sonntag, J.: Sea ice thickness, freeboard, and snow depth products from Operation IceBridge airborne data, The Cryosphere, 7, 1035–1056, 2013.

Kurtz, N., M. Studinger, J., Harbeck, V., Onana, V., and Yi, D.: IceBridge L4 Sea Ice Freeboard, Snow Depth, and Thickness, Version 1, https://doi.org/10.5067/G519SHCKWQV6, 2015.

Kurtz, N., M. Studinger, J., Harbeck, V., Onana, V., and Yi, D.: IceBridge Sea Ice Freeboard, Snow Depth, and Thickness Quick Look, Version 1, https://doi.org/10.5067/GRIXZ91DE0L9, 2016.

Kurtz, N. T. and Farrell, S. L.: Large-scale surveys of snow depth on Arctic sea ice from Operation IceBridge, Geophysical Research Letters, 38, 2011.

Kwok, R.: Arctic sea ice thickness, volume, and multiyear ice coverage: losses and coupled variability (1958–2018), Environmental Research Letters, 13, 105 005, 2018.

Landy, J., Dawson, G., Tsamados, M., and et al: A year-round satellite sea-ice thickness record from CryoSat-2, Nature, 2022.

Landy, J. C., de Rijke-Thomas, C., Nab, C., Lawrence, I., Glissenaar, I. A., Mallett, R. D., Fredensborg Hansen, R. M., Petty, A., Tsamados, M., Macfarlane, A. R., et al.: Anticipating CRISTAL: An exploration of multi-frequency satellite altimeter snow depth estimates over Arctic sea ice, 2018–2023, EGUsphere, 2024, 1–41, 2024.

Laxon, S. W., Giles, K. A., Ridout, A. L., Wingham, D. J., Willatt, R., Cullen, R., Kwok, R., Schweiger, A., Zhang, J., Haas, C., et al.: CryoSat-2 estimates of Arctic sea ice thickness and volume, Geophysical Research Letters, 40, 732–737, 2013.

Lipscomb, W. H.: Remapping the thickness distribution in sea ice models, Journal of Geophysical Research: Oceans, 106, 13 989–14 000, 2001.

Lipscomb, W. H. and Hunke, E. C.: Modeling sea ice transport using incremental remapping, Monthly weather review, 132, 1341–1354, 2004.

Lipscomb, W. H., Hunke, E. C., Maslowski, W., and Jakacki, J.: Ridging, strength, and stability in high-resolution sea ice models, Journal of Geophysical Research: Oceans, 112, 2007.

Massonnet, F., Fichefet, T., and Goosse, H.: Prospects for improved seasonal Arctic sea ice predictions from multivariate data assimilation, Ocean Modelling, 88, 16–25, 2015.

Melia, N., Haines, K., and Hawkins, E.: Sea ice decline and 21st century trans-Arctic shipping routes, Geophysical Research Letters, 43, 9720–9728, 2016.

Mignac, D., Martin, M., Fiedler, E., Blockley, E., and Fournier, N.: Improving the Met Office's Forecast Ocean Assimilation Model (FOAM) with the assimilation of satellite-derived sea-ice thickness data from CryoSat-2 and SMOS in the Arctic, Quarterly Journal of the Royal Meteorological Society, 2022.

Min, C., Yang, Q., Chen, D., Yang, Y., Zhou, X., Shu, Q., and Liu, J.: The emerging Arctic shipping corridors, Geophysical Research Letters, 49, e2022GL099 157, 2022.

Min, C., Yang, Q., Luo, H., Chen, D., Krumpen, T., Mamnun, N., Liu, X., and Nerger, L.: Improving Arctic sea-ice thickness estimates with the assimilation of CryoSat-2 summer observations, Ocean-Land-Atmosphere Research, 2, 0025, 2023.

Mu, L., Yang, Q., Losch, M., Losa, S. N., Ricker, R., Nerger, L., and Liang, X.: Improving sea ice thickness estimates by assimilating CryoSat-2 and SMOS sea ice thickness data simultaneously, Quarterly Journal of the Royal Meteorological Society, 144, 529–538, 2018.

https://doi.org/10.5194/egusphere-2026-742
Preprint. Discussion started: 23 February 2026

Mu, L., Nerger, L., Tang, Q., Loza, S. N., Sidorenko, D., Wang, Q., Semmler, T., Zampieri, L., Losch, M., and Goessling, H. F.: Toward a data assimilation system for seamless sea ice prediction based on the AWI climate model, Journal of Advances in Modeling Earth Systems, 12, e2019MS001 937, 2020.

Nab, C., Mignac, D., Landy, J., Martin, M., Stroeve, J., and Tsamados, M.: Sensitivity to sea ice thickness parameters in a coupled ice-ocean data assimilation system, Journal of Advances in Modeling Earth Systems, 17, e2024MS004 276, 2025.

Nerger, L. and Hiller, W.: Software for ensemble-based data assimilation systems—Implementation strategies and scalability, Computers & Geosciences, 55, 110–118, 2013.

Nerger, L., Hiller, W., and Schröter, J.: PDAF-the parallel data assimilation framework: experiences with Kalman filtering, in: Use of high performance computing in meteorology, pp. 63–83, World Scientific, 2005.

Notz, D. and Stroeve, J.: Observed Arctic sea-ice loss directly follows anthropogenic CO2 emission, Science, 354, 747–750, 2016.

Pham, D. T., Verron, J., and Roubaud, M. C.: A singular evolutive extended Kalman filter for data assimilation in oceanography, Journal of Marine systems, 16, 323–340, 1998.

Previdi, M., Smith, K. L., and Polvani, L. M.: Arctic amplification of climate change: a review of underlying mechanisms, Environmental Research Letters, 16, 093 003, 2021.

Pringle, D., Eicken, H., Trodahl, H., and Backstrom, L.: Thermal conductivity of landfast Antarctic and Arctic sea ice, Journal of Geophysical Research: Oceans, 112, 2007.

Rampal, P., Bouillon, S., Ólason, E., and Morlighem, M.: neXtSIM: a new Lagrangian sea ice model., Cryosphere Discussions, 9, 2015.

Rantanen, M., Karpechko, A. Y., Lipponen, A., Nordling, K., Hyvärinen, O., Ruosteenoja, K., Vihma, T., and Laaksonen, A.: The Arctic has warmed nearly four times faster than the globe since 1979, Communications Earth & Environment, 3, 168, 2022.

Ricker, R., Hendricks, S., Helm, V., Skourup, H., and Davidson, M.: Sensitivity of CryoSat-2 Arctic sea-ice freeboard and thickness on radar-waveform interpretation, The Cryosphere, 8, 1607–1622, 2014.

Ricker, R., Hendricks, S., Kaleschke, L., Tian-Kunze, X., King, J., and Haas, C.: A weekly Arctic sea-ice thickness data record from merged CryoSat-2 and SMOS satellite data, The Cryosphere, 11, 1607–1623, 2017.

Riihelä, A., Bright, R. M., and Anttila, K.: Recent strengthening of snow and ice albedo feedback driven by Antarctic sea-ice loss, Nature Geoscience, 14, 832–836, 2021.

Rolph, R. J., Feltham, D. L., and Schröder, D.: Changes of the Arctic marginal ice zone during the satellite era, The Cryosphere, 14, 1971–1984, 2020.

Rostosky, P., Spreen, G., Farrell, S. L., Frost, T., Heygster, G., and Melsheimer, C.: Snow depth retrieval on Arctic sea ice from passive microwave radiometers—Improvements and extensions to multiyear ice using lower frequencies, Journal of Geophysical Research: Oceans, 123, 7120–7138, 2018.

Rothrock, D., Percival, D., and Wensnahan, M.: The decline in arctic sea-ice thickness: Separating the spatial, annual, and interannual variability in a quarter century of submarine data, Journal of Geophysical Research: Oceans, 113, 2008.

Rothrock, D. A.: The energetics of the plastic deformation of pack ice by ridging, Journal of Geophysical Research, 80, 4514–4519, 1975.

Sakov, P., Counillon, F., Bertino, L., Lisæter, K., Oke, P., and Korablev, A.: TOPAZ4: an ocean-sea ice data assimilation system for the North Atlantic and Arctic, Ocean Science, 8, 633–656, 2012.

Schröder, D., Feltham, D. L., Tsamados, M., Ridout, A., and Tilling, R.: New insight from CryoSat-2 sea ice thickness for sea ice modelling, The Cryosphere, 13, 125–139, 2019.

https://doi.org/10.5194/egusphere-2026-742
Preprint. Discussion started: 23 February 2026

Schuur, E. A., Abbott, B. W., Commane, R., Ernakovich, J., Euskirchen, E., Hugelius, G., Grosse, G., Jones, M., Koven, C., Leshyk, V., et al.: Permafrost and climate change: Carbon cycle feedbacks from the warming Arctic, Annual Review of Environment and Resources, 47, 343–371, 2022.

Schweiger, A., Lindsay, R., Zhang, J., Steele, M., Stern, H., and Kwok, R.: Uncertainty in modeled Arctic sea ice volume, Journal of Geophysical Research: Oceans, 116, 2011.

Shu, Y., Cui, H., Song, L., Gan, L., Xu, S., Wu, J., and Zheng, C.: Influence of sea ice on ship routes and speed along the Arctic Northeast Passage, Ocean & Coastal Management, 256, 107 320, 2024.

Stroeve, J. and Notz, D.: Changing state of Arctic sea ice across all seasons, Environmental Research Letters, 13, 103 001, 2018.

Stroeve, J., Nandan, V., Willatt, R., Tonboe, R., Hendricks, S., Ricker, R., Mead, J., Mallett, R., Huntemann, M., Itkin, P., et al.: Surface-based Ku-and Ka-band polarimetric radar for sea ice studies, The Cryosphere, 14, 4405–4426, 2020.

Stroeve, J. C., Markus, T., Boisvert, L., Miller, J., and Barrett, A.: Changes in Arctic melt season and implications for sea ice loss, Geophysical Research Letters, 41, 1216–1225, 2014.

Strong, C., Foster, D., Cherkaev, E., Eisenman, I., and Golden, K. M.: On the definition of marginal ice zone width, Journal of Atmospheric and Oceanic Technology, 34, 1565–1584, 2017.

Sumata, H., De Steur, L., Divine, D. V., Granskog, M. A., and Gerland, S.: Regime shift in Arctic Ocean sea ice thickness, Nature, 615, 443–449, 2023.

Thomas, D. and Rothrock, D.: The Arctic Ocean ice balance: A Kalman smoother estimate, Journal of Geophysical Research: Oceans, 98, 10 053–10 067, 1993.

Thomas, D., Martin, S., Rothrock, D., and Steele, M.: Assimilating satellite concentration data into an Arctic sea ice mass balance model, 1979–1985, Journal of Geophysical Research: Oceans, 101, 20 849–20 868, 1996.

Tilling, R. L., Ridout, A., and Shepherd, A.: Estimating Arctic sea ice thickness and volume using CryoSat-2 radar altimeter data, Advances in Space Research, 62, 1203–1225, 2018.

Tsamados, M., Feltham, D. L., and Wilchinsky, A.: Impact of a new anisotropic rheology on simulations of Arctic sea ice, Journal of Geophysical Research: Oceans, 118, 91–107, 2013.

Tsamados, M., Feltham, D. L., Schroeder, D., Flocco, D., Farrell, S. L., Kurtz, N., Laxon, S. W., and Bacon, S.: Impact of variable atmospheric and oceanic form drag on simulations of Arctic sea ice, Journal of Physical Oceanography, 44, 1329–1353, 2014.

Warren, S. G., Rigor, I. G., Untersteiner, N., Radionov, V. F., Bryazgin, N. N., Aleksandrov, Y. I., and Colony, R.: Snow depth on Arctic sea ice, Journal of Climate, 12, 1814–1829, 1999.

West, A. E. and Blockley, E. W.: CMIP6 models overestimate sea ice melt, growth & conduction relative to ice mass balance buoy estimates, Geoscientific Model Development Discussions, 2024, 1–33, 2024.

Williams, N., Byrne, N., Feltham, D., Van Leeuwen, P. J., Bannister, R., Schroeder, D., Ridout, A., and Nerger, L.: The effects of assimilating a sub-grid-scale sea ice thickness distribution in a new Arctic sea ice data assimilation system, The Cryosphere, 17, 2509–2532, 2023.

Williams, N., Wang, Y., and Counillon, F.: Enhancing sea ice knowledge through assimilation of sea ice thickness from ENVISAT and CS2SMOS, EGUsphere, 2025, 1–29, 2025.

Wingham, D., Francis, C., Baker, S., Bouzinac, C., Brockley, D., Cullen, R., de Chateau-Thierry, P., Laxon, S., Mallow, U., Mavrocordatos, C., et al.: CryoSat: A mission to determine the fluctuations in Earth's land and marine ice fields, Advances in Space Research, 37, 841–871, 2006.

https://doi.org/10.5194/egusphere-2026-742
Preprint. Discussion started: 23 February 2026

Xie, J., Counillon, F., and Bertino, L.: Impact of assimilating a merged sea-ice thickness from CryoSat-2 and SMOS in the Arctic reanalysis, The Cryosphere, 12, 3671–3691, 2018.

Yang, Q., Losa, S. N., Losch, M., Tian-Kunze, X., Nerger, L., Liu, J., Kaleschke, L., and Zhang, Z.: Assimilating SMOS sea ice thickness into a coupled ice-ocean model using a local SEIK filter, Journal of Geophysical Research: Oceans, 119, 6680–6692, 2014.

Zhang, J. and Rothrock, D. A.: Modeling global sea ice with a thickness and enthalpy distribution model in generalized curvilinear coordinates, Monthly Weather Review, 131, 845–861, 2003.

Zhang, Y.-F., Bushuk, M., Winton, M., Hurlin, B., Gregory, W., Landy, J., and Jia, L.: Improvements in September Arctic Sea Ice Predictions Via Assimilation of Summer CryoSat-2 Sea Ice Thickness Observations, Geophysical Research Letters, 50, e2023GL105 672, 2023.